UNITED NATIONS EDUCATIONAL, SCIENTIFIC AND CULTURAL ORGANIZATION
INTERNATIONAL ATOMIC ENERGY AGENCY
INTERNATIONAL CENTRE FOR THEORETICAL PHYSICS
I.C.T.P., P.O. BOX 586, 34100 TRIESTE, ITALY, CABLE: CENTRATOM TRIESTE

SMR/989 - 3

"Course on Shallow Water and Shelf Sea Dynamics "
7 - 25 April 1997

"Tides in the Strait of Gibraltar"

J. CANDELA
Centro de Investigacion Cientifica
Y Educacion Superior de Ensenada (Cicese)
Ensenada
Mexico

JOURNAL OF GEOPHYSICAL RESEARCH, VOL. 95, NO. C5, PAGES 7313–7335, MAY 15, 1990

Tides in the Strait of Gibraltar

JULIO CANDELA AND CLINTON WINANT

Scripps Institution of Oceanography, La Jolla, California

ANTONIO RUIZ

Instituto Hidrográfico de la Marina, Cadiz, Spain

The Strait of Gibraltar is where the transition occurs between two distinct tidal regimes: the North Atlantic, where tidal ranges are in excess of 2 m, and the western Mediterranean, where tidal ranges are less than 1 m. Within the strait the tide is principally semidiurnal: observations indicate that on average, 96% of the bottom pressure and 74% of the current variability are contained in the semidiurnal band (2 cpd). The structure of the local cotidal chart of the M_2 tidal constituent is complicated but can be explained in terms of the along- and across-strait momentum balances. Along the strait, the pressure gradient is mainly balanced by the acceleration of the flow, although friction can be of appreciable magnitude, corresponding to a decay time scale of 3–16 hours. Across the strait the momentum balance appears mostly geostrophic, but better observations would be required to explain residual terms. Available observations indicate that the M_2 tide has no net energy flux through the strait. At the sill the tidal transport in the upper layer exceeds that in the lower layer by nearly a factor of 2. At the eastern end of the strait, between Algeciras and Ceuta, the tidal transport is larger in the lower layer. This apparent shift in the location of maximum tidal transport is explained in terms of the kinematics of the interface between Atlantic and Mediterranean waters. A mean transport of 0.21 Sv, due to subinertial and tidal flows, carries Atlantic water through the strait, compensated by an approximately equal return in the lower layer.

1. INTRODUCTION

The North Atlantic Ocean connects with the Mediterranean Sea through the Strait of Gibraltar. The strait has a length of nearly 60 km, and at its most narrow section (Point Cires section) the width is 12 km (Figure 1). The sill, located between Punta Paloma (Spain) and Punta Altares (Morocco) is a prominent feature in the strait. It has a maximum depth of 300 m. East of the sill the channel deepens to nearly 600 m at the Tarifa section, and to 900 m at the Algeciras-Ceuta section. West of the sill the depth reaches 450 m north of Tangier, but further west a secondary sill in front of Cape Spartel is shallower (nearly 350 m), and then the depth increases gradually down toward the deep North Atlantic.

Lacombe and Richez [1982] have suggested that the flow variability through the strait can be categorized into three distinct types: long-term, subinertial, and tidal. The long-term flow exhibits seasonal and interannual variability and relates to the two-layer baroclinic exchange with Atlantic waters flowing into the Mediterranean at the surface and Mediterranean waters flowing out into the Atlantic near the bottom. Fluctuations in the evaporation-precipitation budget over the Mediterranean Sea, deep water formation processes, and seasonal winds are factors which have been shown to influence the long-term variability of the exchange in models proposed by *Bryden and Stommel* [1984] and *Bormans et al.* [1986]. Recently, *Farmer and Armi* [1986] proposed a hydraulic control theory applicable to the mean exchange, which raises the possibility of having a maximal mean exchange condition in the strait at all times. Subinertial flows, with periods ranging from days to a few months, are mostly barotropic with root-mean-squared transport values of nearly 0.4 Sv, and have been found to be principally forced by the atmospheric pressure field over the Mediterranean [*Candela et al.*, 1989]. Tidal flows are also for the most part barotropic in the strait and are principally driven by the North Atlantic tide. These provide the central focus of this paper.

Although conceptually simple, this classification of the flow through the strait does not account for the appreciable nonlinear interactions which can occur between the different flow regimes. In particular, the high correlation found between depth fluctuations of the interface separating the Atlantic and Mediterranean waters, and barotropic flows at the sill, both at tidal and subinertial frequencies, imply appreciable net transports [*Bryden et al.*, 1988; *Candela et al.*, 1989].

As the tidal ranges in the North Atlantic exceed 2 m, while in the Mediterranean the ranges are less than 1 m, a drastic transition in the tides must occur within the strait. Extensive surveys carried out between 1960 and 1967 resulted in the first description of the complicated tidal characteristics in this area [*Lacombe and Richez*, 1982]. Here recent observations made in the course of the Gibraltar Experiment [*Kinder and Bryden*, 1987] are used, first to describe the tidal motions in the strait and then to give both a kinematic and a dynamic interpretation when observations are sufficient to allow these to be made.

2. TIDAL OBSERVATIONS

In the course of the Gibraltar Experiment, which took place between October of 1985 and October of 1986, currents, pressure, salinity, and temperature time series were obtained at different locations in the strait with moored as well as bottom-mounted instruments. Nine bottom pressure instruments and 11 current meter mooring locations were occupied, as shown in Figure 1. Tables 1 and 2 summarize deployment information for bottom pressure and current meter moorings.

Three characteristic bottom pressure observations for the western (DW), main sill (SN), and eastern (CE) sites are illustrated in Figure 2*a*, for the four-month period extending from November 5, 1985, to March 5, 1986. The time series have a strong semidiurnal character, with a correspondingly marked fort-

Paper number 89JC03176.
0148-0227/90/89JC-03176$05.00

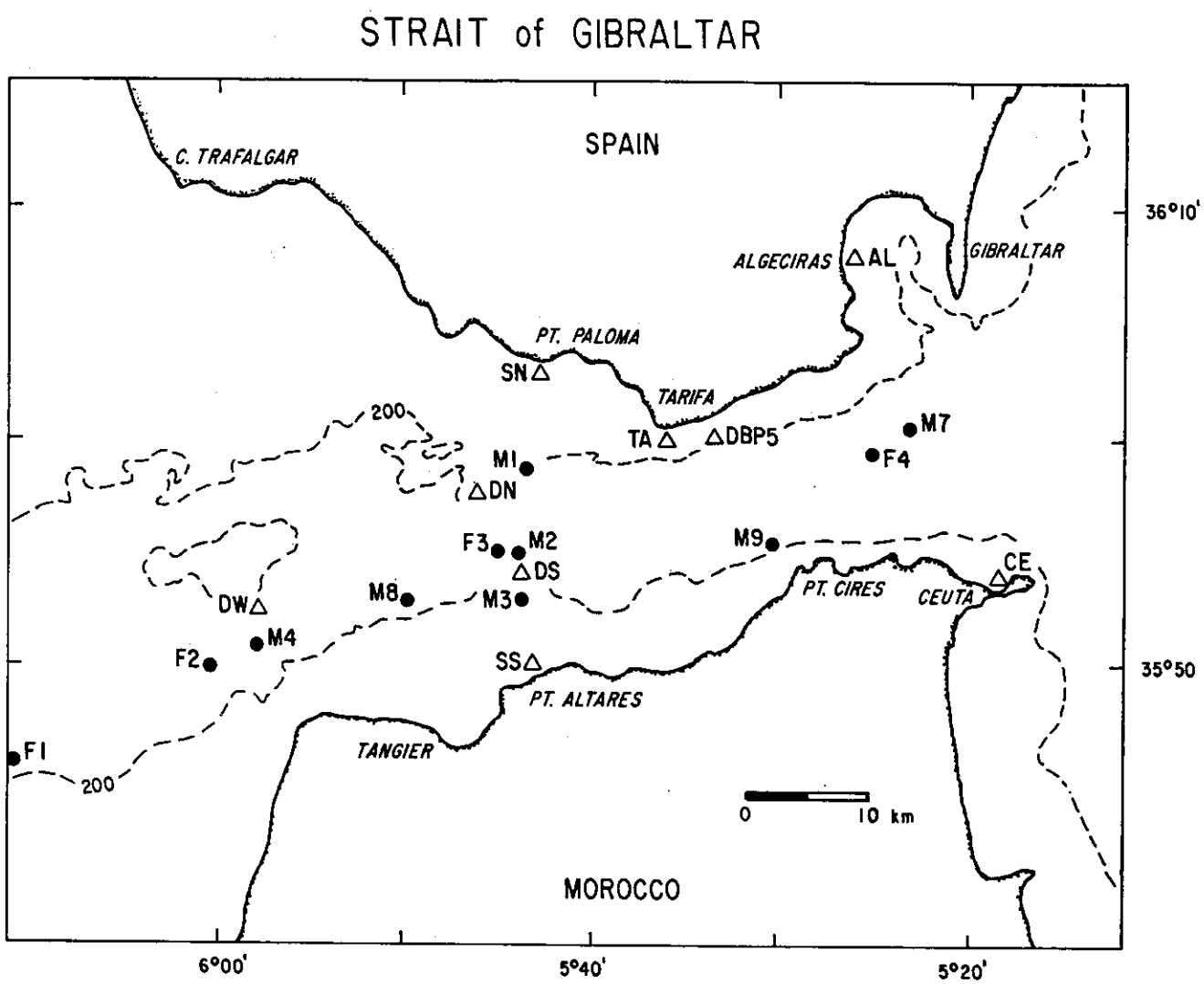

Fig. 1. Map of the Strait of Gibraltar showing locations referred to in the text. Also shown are the location of the bottom pressure sensors (triangles) and the current meter moorings (solid circles) deployed during the Gibraltar Experiment (October 1985 to October 1986).

TABLE 1. Information for the Pressure Measurements During the Gibraltar Experiment

Station	Depth, m	Latitude North	Longitude West	Start	Stop	Type of Instrument
DW	260	35°53'	05°58'	October 25, 1985	March 17, 1986	BP.SIO
SN	11	36°03'	05°43'	October 22, 1985	January 26, 1986	BP.SIO
				March 4, 1986	August 6, 1986	
DN	210	35°58'	05°46'	October 26, 1985	March 3, 1986	BP.SIO
DS	210	35°54'	05°44'	October 27, 1985	March 21, 1986	BP.SIO
SS	12	35°50'	05°43'	April 17, 1986	August 20, 1986	BP.SIO
DP5	160	36°00'	05°34'	October 19, 1985	March 19, 1986	BP.UNH
TA	5	36°01'	05°36'	October 10, 1985	November 14, 1985	AA.IHM
				December 16, 1985	February 20, 1986	
				March 11, 1986	July 16, 1986	
AL	5	36°08'	05°26'	October 10, 1985	May 1, 1986	AA.IHM
				May 12, 1986	June 26, 1986	
CE	5	35°53'	05°18'	October 18, 1985	May 9, 1986	AA.IHM
				January 1, 1986	August 7, 1986	STG.IHM

Abbreviations are as follows: DW, Deep West; SN, Shallow North; DN, Deep North; DS, Deep South; SS, Shallow South; DP5, Doppler acoustic logger #5; TA, Tarifa; AL, Algeciras; CE, Ceuta; BP.SIO, bottom pressure from Scripps; BP.UNH, bottom pressure from the University of New Hampshire; AA.IHM, Aanderaa bottom pressure from Instituto Hidrográfico de la Marina (IHM); STG.IHM, Standard tide gauge from IHM. The deep bottom pressure measurement south of Tarifa DP5 was provided by Neal Pettigrew from the University of New Hampshire.

TABLE 2*a*. Information for Current Meter Moorings During First Deployment of the Gibraltar Experiment

Station	Water Depth, m	Latitude North	Longitude West	Start	Stop	Depth of Instrument, m
M1	222	35°58.26'	05°44.62'	October 22, 1985	May 4, 1986	143
				October 22, 1985	May 4, 1986	156
				October 22, 1985	May 4, 1986	167
				October 22, 1985	May 4, 1986	215
M2	321	35°54.79'	05°44.41'	October 22, 1985	November 23, 1985	123
				October 22, 1985	November 23, 1985	143
				October 22, 1985	November 23, 1985	153
				October 22, 1985	November 23, 1985	191*
				October 22, 1985	November 23, 1985	254
				October 22, 1985	November 23, 1985	306
M3	190	35°53.42'	05°44.20'	October 21, 1985	April 21, 1986	110
				October 21, 1985	April 21, 1986	140
				October 21, 1985	April 21, 1986	180
M4	358	35°51.68'	05°58.64'	October 17, 1985	November 9, 1985	67
M7	916	35°59.98'	05°22.75'	October 19, 1985	March 27, 1986	54
				October 19, 1985	March 27, 1986	193
M8	610	35°53.16'	05°50.55'	October 17, 1985	March 26, 1986	30

Mooring name, water depth, location, start and stop times of observation and nominal depth or minimum depth recorded by instrument when equipped with pressure sensor are indicated. Measurements provided by H. Bryden from Woods Hole Oceanographic Institution (WHOI) and described by *Pillsbury et al.* [1987].

*This instrument had a malfunctioning rotor and did not record speed, but the direction, pressure, temperature, and conductivity records are of good quality.

TABLE 2*b*. Information for Current Meter Moorings During Second Deployment of the Gibraltar Experiment

Station	Water Depth, m	Latitude North	Longitude West	Start	Stop	Depth of Instrument, m
M2	310	35°54.74'	05°44.55'	May 29, 1986	August 19, 1986	90
				May 29, 1986	October 13, 1986	112*
				May 29, 1986	October 13, 1986	135*
				May 29, 1986	October 13, 1986	181*
				May 29, 1986	October 13, 1986	233*
				May 29, 1986	October 13, 1986	299*
M3	183	35°53.42'	05°44.22'	May 28, 1986	June 23, 1986	102
				May 28, 1986	June 20, 1986	127
				May 28, 1986	June 26, 1986	172
M4	354	35°52.07'	05°57.03'	May 29, 1986	October 13, 1986	340
M9	170	35°55.23'	05°29.98'	May 28, 1986	October 13, 1986	58*
				May 28, 1986	October 13, 1986	159

Measurements provided by H. Bryden of WHOI and discussed by *Pillsbury et al.* [1987].

*These instruments had problems with the current sensing device and have current records shorter than the time between start and stop shown, although the other parameters were recorded properly over this period.

TABLE 2*c*. Information for the Current Meter Moorings Deployed During April 1986

Station	Water Depth, m	Latitude North	Longitude West	Start	Stop	Depth of Instrument, m
F1	400	35°45.40'	06°20.93'	April 7, 1986	April 21, 1986	204*
				April 7, 1986	April 21, 1986	260*
				April 7, 1986	April 21, 1986	320
				April 7, 1986	April 21, 1986	380
F2	350	35°50.85'	06°00.50'	April 5, 1986	April 23, 1986	220*
				April 5, 1986	April 23, 1986	280*
				April 5, 1986	April 23, 1986	320
F3	300	35°55.30'	05°44.80'	April 7, 1986	April 24, 1986	63*
				April 7, 1986	April 24, 1986	126*
				April 7, 1986	April 24, 1986	165
				April 7, 1986	April 24, 1986	225
F4	890	35°59.00'	05°25.80'	April 8, 1986	April 19, 1986	60*
				April 8, 1986	April 19, 1986	120*

Measurements provided by D. Farmer, Institute of Ocean Sciences, Patricia Bay, Sidney, British Columbia.
*Instruments equipped with pressure sensors; depths indicated are minimum depths recorded.

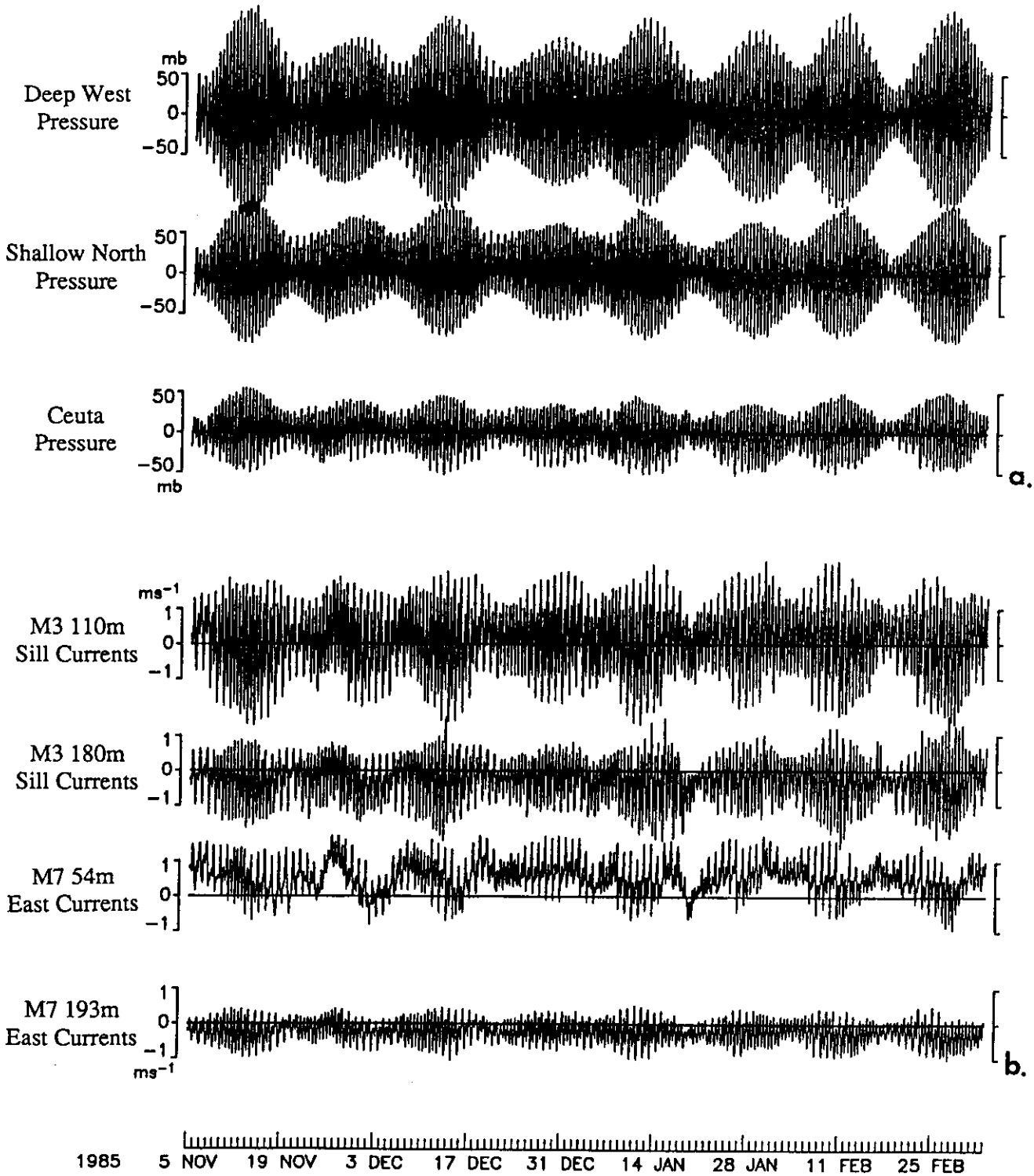

Fig. 2. Characteristic bottom pressure and current observations obtained during the experiment. (*a*) Bottom pressure observations for three locations along the strait's axis at the western (Deep West, DW in Figure 1) main sill (Shallow North, SN) and eastern end (Ceuta, CE). (*b*) Principal axis currents observed at the sill (M3 at 110-m and 180-m depth) and at the eastern end (M7 at 54-m and 193-m depth). Positive currents are toward the Mediterranean. The mean of each series is M3-110 m, 0.10 m s^{-1}; M3-180 m, -0.25 m s^{-1}; M7-54 m, 0.54 m s^{-1}; and M7-193 m, -0.22 m s^{-1}. The time series shown cover a period of 4 months, from November 5, 1985, to March 5, 1986, as indicated by the time axis at the bottom of the figure.

nightly modulation due to the beating of the two dominant semidiurnal tidal constituents, M_2 and S_2. Power spectra, calculated with a broad frequency band resolution of 1 cpd, indicate that 96.1% of the pressure field variance is contained in the semidiurnal band (2 cpd), while low frequencies account for only 1.6% of the variance and the diurnal band accounts for 1%. These represent an average energy distribution for the nine pressure stations available and the distribution of variance for individual stations does not vary much from the average distribution. The series illustrated in Figure 2*a* show a marked reduction in amplitude between the western and eastern ends of the strait. This reflects the matching of the different tidal characteristics from the

Atlantic to the Mediterranean side and results from the strong reflection of the tidal wave which enters from the Atlantic, as described further. Currents in the strait also exhibit strong semidiurnal fluctuations as illustrated in Figure 2*b*. Currents are strongly polarized in the strait, and it is practical to decompose horizontal currents at any location in terms of fluctuations along principal axes. Major axis component currents at four sites are illustrated in Figure 2*b*, two sites are at the main sill (mooring M3 at depths of 110 m and 180 m), and the other two sites are at the eastern end of the strait (mooring M7 at 54-m and 193-m depth). Mean and vector power spectra calculations for all the available current meter measurements are summarized in Table 3. Average spectra of currents in the strait show that 6.6% of the variance occurs at low frequencies with periods longer than 1 day, 11.6% of the variance occurs at the diurnal frequencies, and 74% of the variance is associated with semidiurnal period fluctuations. In general, the amplitude of the current decreases with increasing depth and with distance east of the sill. An exception to this general behavior is found in the upper layer at the eastern end, where 52% of the energy occurs at low frequencies, 20% of the energy occurs at diurnal frequencies, and 19% occurs in the semidiurnal frequency band. This energy distribution is only observed in the upper layer at mooring M7. On the same mooring in the lower layer the energy distribution for currents is similar to that of other measurements in the strait. All observations, since those reported by *Lacombe and Richez* [1982] have shown that the depth of the upper layer decreases toward the east. As a result, the increase in energy for low-frequency and subinertial flows is expected from simple continuity considerations. The relative decrease in energy at tidal periods seems surprising but can be explained in terms of a kinematic model of the interface described further. West of the sill there is a tendency for the mean, subinertial and diurnal currents to be stronger at depth, as indicated by the measurements on moorings M4, F1, and F2 (Table 3). West of the sill, the thickness of the lower layer is reduced and the current variability shifts toward lower frequencies. This behavior is reversed in the east.

This overview of pressure and current observations shows how the tidal motions are an essential feature of the exchange in the

TABLE 3. Mean Current and Vector Power Spectra Calculations

		Length	Mean		Frequency Band ($\Delta\sigma$ = 1 cpd)								
	Depth,	of series,	Amplitude,	Orientation,	Subinertial			Diurnal			Semidiurnal		
Station	m	hours	cm s^{-1}	deg	M, cm s^{-1}	m, cm s^{-1}	θ, deg	M, cm s^{-1}	m, cm s^{-1}	θ, deg	M, cm s^{-1}	m, cm s^{-1}	θ, deg
M1	143	4657	16	-144	31	1	-5	35	-1	-11	92	-6	-8
	156	4157	19	-164	28	1	-18	32	-1	-26	86	-6	-20
	167	4649	20	-150	27	1	-8	31	-2	-16	83	-6	-9
	215	4657	12	168	14	1	-21	16	0	-17	48	-2	-16
M2	90	1974	14	-8	38	-2	12	53	0	18	130	1	7
	112	745	2	174	28	-5	25	48	-3	24	127	-2	12
	123	766	11	-117	46	-1	13	49	0	11	130	-4	12
	135	1980	30	-153	26	0	11	43	-1	16	126	-8	16
	143	766	17	-150	33	1	5	47	0	13	116	-5	12
	153	766	28	-147	35	1	10	51	-2	13	127	-8	15
	181	990	51	-158	23	4	12	45	-3	14	100	-14	20
	233	2200	64	-160	23	2	45	33	1	24	77	0	26
	254	766	53	-150	18	0	25	35	1	26	88	1	30
	299	620	46	-146	11	3	37	25	0	39	59	1	41
	306	766	38	-134	18	-1	18	29	1	41	65	2	43
M3	102	631	16	36	23	0	-4	44	2	-2	105	-3	6
	110	4358	13	51	43	0	-9	48	3	6	123	-3	9
	127	545	11	36	20	1	-12	40	5	-4	90	-5	12
	140	4358	6	138	38	1	-2	40	1	6	111	-5	12
	172	687	7	-161	14	0	9	21	1	13	51	-1	19
	180	4358	25	-157	27	-1	19	26	0	20	71	-4	22
M4	67	537	25	20	10	-1	22	17	0	27	47	0	16
	340	3274	88	-168	23	-1	12	19	-1	25	28	-6	33
M7	54	3808	54	7	55	2	10	30	-6	9	36	-5	14
	193	3808	22	-152	15	-1	35	16	1	25	39	2	26
M8	30	3166	37	13	21	-1	27	28	2	23	71	2	14
M9	58	2060	59	8	25	1	16	28	-3	8	53	2	13
	159	3316	30	34	26	0	18	23	-1	16	65	1	17
F1	204	332	19	15	7	-1	-51	5	-2	9	15	-4	11
	260	330	26	25	12	-4	42	7	-1	33	16	-4	16
	320	332	23	171	16	-1	6	7	1	12	22	0	25
	380	332	146	-154	10	0	55	32	0	-67	12	0	60
F2	220	421	4	-123	17	1	12	14	-1	29	22	0	26
	280	421	94	-151	42	0	31	48	-1	28	61	0	28
	320	421	165	-158	13	-2	-1	14	-1	-8	33	-3	16
F3	63	403	21	-18	41	-1	24	44	0	19	112	3	12
	126	403	36	142	31	0	13	49	-1	14	117	-5	16
	165	403	53	-143	35	1	39	26	0	27	79	-5	29
	225	403	60	-137	29	1	36	27	-1	39	81	0	40
F4	60	254	28	12	25	-2	13	31	-5	13	48	-2	23
	120	254	16	-163	11	0	23	12	-1	21	35	-1	19

Spectral estimates are for a frequency band resolution of 1 cpd and are expressed by the ellipse parameters of the first 3 bands resolved, i.e., subinertial, diurnal, and semidiurnal. M is the semimajor axis, m is the semiminor axis, and θ is the orientation in degrees with respect to east. The sign of the semiminor axis indicates the mean sense of rotation of the currents within the band, positive values implying a counterclockwise mean rotation. Information for the two deployment times for moorings M2 and M3 has been merged in one column according to instrument depth.

TABLE 4. Principal Tidal Constituents for the Pressure Records

Station	Length of Series, hours	Diurnal Band O_1 Amplitude	O_1 Phase	K_1 Amplitude	K_1 Phase	Semidiurnal Band M_2 Amplitude	M_2 Phase	S_2 Amplitude	S_2 Phase
DW	3414	4.7	$300.6°_{+}$	4.7	$47.1°_{+}$	78.5	$56.1°_{+}$	29.0	$82.2°_{DN}$
SN	3464	0.7	$298.0°_{+}$	2.1	$95.3°_{+}$	52.3	$47.6°_{+}$	18.5	$73.4°_{DN}$
DN*	3257	1.5	$291.7°_{+}$	2.5	$83.3°_{+}$	60.1	$51.8°_{+}$	22.5	$73.8°_{+}$
DS*	3459	2.8	$335.7°_{+}$	4.4	$76.3°_{+}$	54.0	$61.8°_{+}$	21.1	$83.3°_{DN}$
SS	2991	3.8	$332.0°_{+}$	5.3	$68.6°_{+}$	57.1	$66.8°_{+}$	20.6	$92.3°_{DN}$
DP5	3406	1.7	$225.3°_{+}$	0.8	$92.2°_{+}$	44.4	$47.6°_{+}$	16.1	$73.9°_{DN}$
TA	3043	1.2	$104.7°_{CE}$	2.1	$145.5°_{CE}$	41.2	$41.2°_{+}$	14.7	$67.9°_{DN}$
AL	4857	1.1	$106.9°_{CE}$	2.1	$147.6°_{CE}$	31.0	$48.0°_{+}$	11.1	$73.9°_{DN}$
CE	8760	2.0	$102.7°_{+}$	3.6	$143.4°_{+}$	29.7	$50.3°_{+}$	11.4	$75.6°_{+}$

Amplitude is in millibars (1 mbar ≈ 1 cm); phase is in degrees with respect to GMT. Subscripts are plus direct harmonic analysis, with inference to separate P_1 from K_1 and K_2 from S_2 using their relation at Cadiz; DN, admittance with deep north predictions; CE, admittance with Ceuta predictions. The specific type of analysis used to obtain the tidal constituents are indicated in each case and explained in the text.

*Corrected for internal contribution. For uncorrected values, see Table 8.

Strait of Gibraltar. It may be expected that through nonlinear interactions the tidal flows can contribute appreciably to mean and subinertial exchanges. In further sections the tidal signal (frequencies greater than 0.5 cpd) is described, and because of the strong dominance of the semidiurnal band, both in pressure and in currents, a detailed description of M_2 tidal constituent is also given. M_2 is the principal lunar semidiurnal constituent at a frequency of 28.98° per hour. In the strait it represents more than 70% of the energy contained in the semidiurnal band and can be taken as the best single frequency representative of the tidal motions.

3. THE SURFACE TIDE IN THE STRAIT

Bottom pressure measurements are dominated by tidal surface fluctuations. However, the internal tide contribution to bottom pressure is appreciable, specially near the sill region. Using density time series from nearby moorings, a correction was performed on the two deep bottom pressure measurements at the sill, i.e., DN and DS. The details of this correction are described in Appendix A. In the analyses which follow, the corrected DN and DS pressure series are used in all the calculations. Series at DW and at DP5 are used as measured with the assumption that the internal contributions are unimportant at these locations. The amplitude and phase of the main tidal constituents in the nine bottom pressure records available are given in Table 4. These have been obtained through direct harmonic analysis and verified by admittance calculations [*Godin*, 1976]. The admittance estimate uses as input reference nearby sea level or bottom pressure stations where more than 6 months of reliable data are available (Cadiz, Ceuta, and DN in this case), such that all the major constituents in the diurnal and semidiurnal bands are resolved.

The ratios and phase differences between the main semidiurnal constituents remain quite constant throughout the strait. This does not hold for the diurnal band where the amplitude ratio and phase difference between its two dominant constituents (O_1 and K_1), differ between the east and west ends of the strait [*García et al.*, 1987; *Garrett et al.*, 1989]. *García et al.* [1987], based on this latter observation, had speculated on the possibility of having an elevation node in the strait for one or both of these diurnal constituents. This speculation would be partly supported by the relatively higher diurnal energy content in the current signal with respect to that in the pressure, as noted in section 2. As explained in Appendix A, the energy content in this band is within the noise level of the observations imposed by the internal tide. The estimates for this band, from direct harmonic analysis or admittance calculations, should be therefore considered cautiously. In the semidiurnal band both methods give close and comparable results, so one can be confident that the amplitude and phase given for M_2 and S_2 are quite stable statistical estimates.

Based on the values listed in Table 4, the cotidal chart for M_2 can be constructed (Figure 3). There are two main features to be noted on this chart. The M_2 amplitude decreases by more than 50% from the Atlantic to the Mediterranean side but is otherwise uniform across the strait. In contrast, the lines of constant phase (cotidal lines) are oriented east-west along the channel, implying ~ 40 min time difference between the time of maximum amplitude at the north and south shores around the Tarifa section. The southward M_2 phase propagation observed in Gibraltar is in clear opposition to the North Atlantic deep water tide west of the strait which propagates northward, with the coast to its right, as expected of a Kelvin wave [*Hendershott*, 1973]. The matching between the North Atlantic and strait M_2 tidal patterns is not clear and requires further consideration. The most reasonable matching

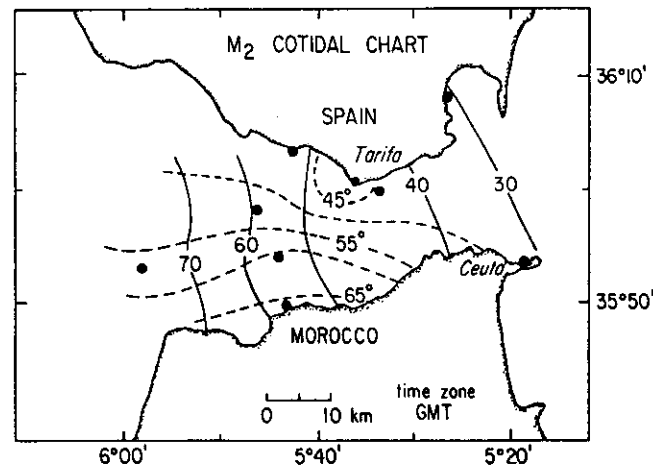

Fig. 3. Cotidal chart for M_2 (frequency = 28.98°/hour), principal lunar semidiurnal tidal constituent. Deduced from analysis of nine bottom pressure stations (solid circles). Amplitude lines (solid lines) are in millibars (1 mbar ~ 1 cm). Phase lines (dashed lines) are in degrees with respect to Greenwich Mean Time.

though, is for phase lines in the strait to close on the Spanish coast, west of the entrance. Insofar as amplitude is concerned, the along-strait gradient adequately matches reports on the Atlantic and Mediterranean sides of the strait [*Sección de Oceanografía*, 1986].

Rocha and Clarke [1987] have considered theoretically the tidal behavior in a strait connecting to semi-infinite oceans. Some of their conclusions are as follows: (1) If the strait is narrow enough (i.e., width (W) << Rossby radius ($Ro = (gh)^{1/2}/f$, where g is the acceleration due to gravity, h is water depth and f is the Coriolis parameter)), sea level tidal constants change linearly from one end to the other, with steep gradients within the strait in the case of differing tides in each ocean. (2) For a short strait (i.e., length/W~1), because of end effects, strong gradients in sea level occur across the strait even when $W << Ro$. (3) The deep sea tide "sees" the strait as a point source at a distance greater than 0.6W from the center point of the entrance to the strait. For Gibraltar, Ro~1000 km, length/W~5, and the tides at both sides differ appreciably, so that the points above seem to apply and give some theoretical explanation to the observed M_2 pattern. The presence of rotational effects on the tides of straits where $W << Ro$, is verified by observations elsewhere [*Godin et al.*, 1981; *Garrett and Petrie*, 1981; *Godin and Candela*, 1987; *Candela and Godin*, 1989], and in some of these places an across-strait geostrophic balance is confirmed.

Our present concern is to compare the pressure and current observations in the strait, so as to estimate the principal dynamical balances that manifest themselves in the pattern illustrated in Figure 3. Even though M_2 accounts for most of the tidal variability observed, restricting a description of the tides to that frequency would imply leaving out subtleties of the tidal behavior due to interactions between constituents in places with complicated topography and large tidal amplitudes such as Gibraltar. To avoid this common bias of just looking at the structure of the predominant constituents, it was also decided to isolate the complete tidal signal in the pressure and currents, by applying the PL64 filter, with a half power point at 38 hours [*Flagg et al.*, 1976], and using the resulting series to investigate the dynamics of the tidal motions in the strait.

Disregarding frictional and nonlinear effects, the along-strait pressure gradient should be balanced by the local acceleration of the flow and the across-strait pressure gradient should be balanced by the flow itself, through geostrophy. If these two balances hold, it may be useful to decompose the pressure field into orthogonal modes, since u and $\partial u/\partial t$ are orthogonal. Also, when intercomparing pressure and/or current observations, as when one evaluates the terms in the momentum equations, it is helpful to isolate that part of the variability which is common to all simultaneous measurements within the study area, from the part which is local or due to individual noise. One method for attaining both goals, i.e., orthogonal modes that also extract the common part from a measured field, is the empirical orthogonal function (EOF) analysis [*Kundu et al.*, 1975]. This type of analysis is thus applied to the pressure data.

Simultaneous high-passed (σ > 0.5 cpd) bottom pressure records are available for eight stations over a 2-month period (December 19, 1985, to February 17, 1986, 1447 hours). Observations for the Shallow South station (SS) are unavailable for this period, but because of its important location it was decided to use predictions obtained using constituents determined from a different time period. The EOF analysis was thus performed with nine simultaneous series of the complete tidal signal.

The first mode that results from the EOF decomposition (Figure 4*a*), represents 97.6% of the tidal variance and consists of a standing wave pattern that has an along-strait amplitude gradient decaying toward the Mediterranean. The spatial weights contoured in Figure 4*a* represent the rms value of the fluctuations of the tide associated with this mode. The second mode (Figure 4*b*) explains only 1.8% of the total variance, and its spatial weights describe an across-strait standing wave with a zero crossing running through the center of the strait. This EOF analysis of the pressure field greatly simplifies the description of the tides in the strait, and just with the use of these two modes it is possible to describe the behavior of any of the principal tidal constituents.

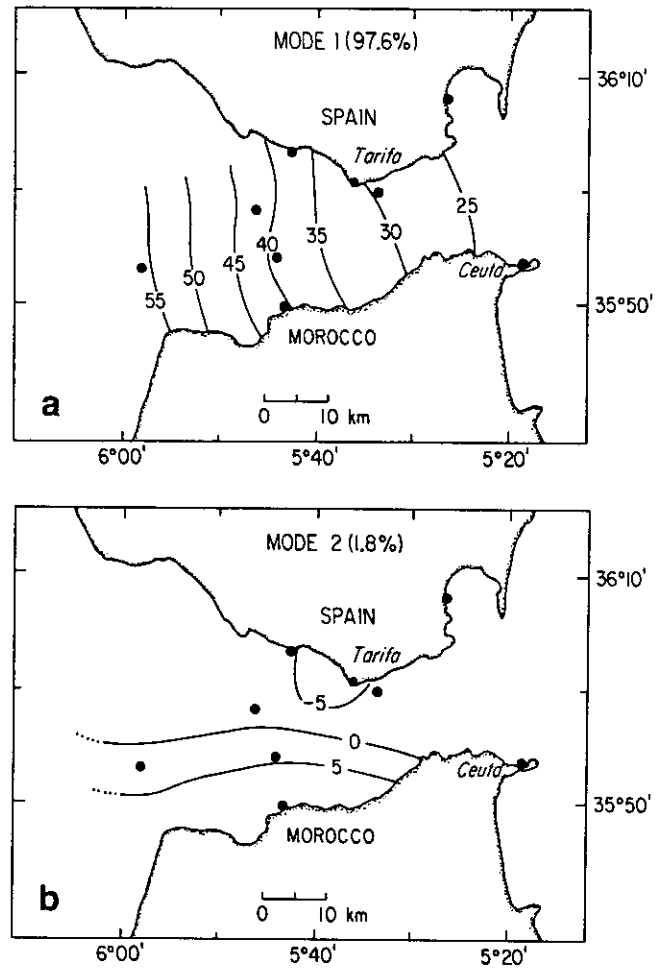

Fig. 4. Empirical orthogonal function (EOF) analysis of the tidal pressure field observed in the strait. (*a*) Contours of the spatial structure of mode 1 representing 97.6% of the total tidal variance. (*b*) Spatial structure of mode 2 representing 1.8% of the variance. Contour values for both modes are in millibars and represent the standard deviation of the pressure field associated with each mode. Nine simultaneous pressure stations (solid circles) covering a period of ~2 months (1447 hours), were used in the analysis.

A harmonic analysis of the time evolution of the two modes (Figure 5) provides the amplitude and phase of the M_2 constituent (or any other principal constituent) associated with each mode. Mode 1 has an M_2 amplitude of 1.37 and a phase of 53.8° and, when multiplied by the weights of Figure 4*a*, gives the main M_2 signal in the strait. The M_2 signal thus obtained shows nearly the same along-strait amplitude gradient as that of Figure 3 but indicates a simultaneous M_2 tide throughout the strait with a phase of 53.8°. The addition of the contribution due to mode 2, with an M_2 amplitude of 1.27 and phase of 142.6°, only slightly alters the

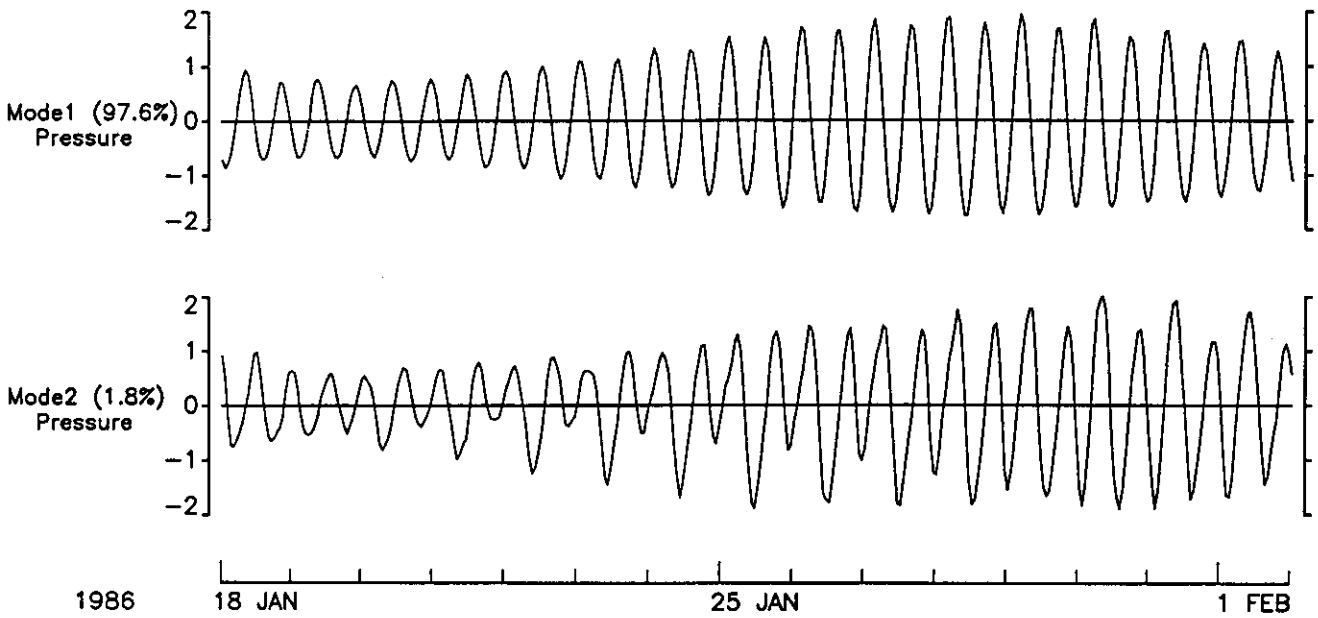

Fig. 5. Series of the time coefficients for the two EOF modes of the pressure field shown in Figure 4. The coefficients are chosen to be dimensionless, but when multiplied with the appropriate spatial weights, reproduce the dimensional time series of the pressure fluctuations due to each mode. Although 2 months of simultaneous observations were used in the analysis, only a 15-day period is shown for clarity.

M_2 amplitude but provides the across-strait phase gradient observed, reproducing the M_2 cotidal chart of Figure 3. This reconstruction of M_2, based on the two principal empirical modes, indicates that at least the spatial structure of these modes could have been deduced directly from the cotidal chart of Figure 3. If instead of plotting the amplitude and phase of M_2 at each location, plots of its real and imaginary parts are made, patterns nearly identical to those of Figures 4*a* and 4*b* are obtained. Both forms of decomposition set the principal tidal field as being composed of two standing wave patterns orthogonal to each other: one with an amplitude gradient along the strait and the other with an across-strait gradient with a zero crossing in the middle.

To determine how these pressure modes are coupled dynamically with the current field, observations from M1, M2, and M3 at the sill section and from M7 at the eastern end are considered. At the sill, moorings M1 and M3 have a common measuring time interval of about 6 months (October 22, 1985, to April 21, 1986). Mooring M1 had four instruments and mooring M3 had three instruments. Mooring M2 broke off after a month but was recovered, with data available from October 22 to November 23,

TABLE 5. High-Pass Currents ($\sigma \geq 1$ cpd)

		Principal Axis Component			EOF	
Mooring	Depth of Instrument, m	Semimajor Orientation, deg	Semiminor Axis, cm s^{-1}	Axis, cm s^{-1}	Mode 1	Mode 2
M1	143	-8.5	71.0	12.1	73.5(67.9)	-14.2(-15.5)
	156	-21.4	66.8	11.6	68.6(64.0)	-20.7(-16.4)
	167	-10.4	64.1	11.9	64.8(61.0)	-21.9(-16.6)
	215	-16.2	37.2	8.4	34.0(33.4)	-16.4(-11.2)
M2	123	12.2	98.9	14.7	96.4	19.8
	143	12.1	89.1	15.5	86.4	17.5
	153	15.3	97.4	16.0	94.8	15.8
	254	29.1	68.8	13.6	65.9	-15.8
	306	41.4	52.4	12.8	48.9	-14.6
M3	110	8.7	92.9	13.2	90.9(90.7)	3.9(16.5)
	140	10.9	83.6	14.3	82.5(81.4)	6.0(15.7)
	180	21.2	55.8	14.1	49.3(51.1)	8.5(14.0)
					92.3%(92.7%)	4.1%(4.9%)
M7	54	10.7	31.0	14.4		
	193	25.9	29.1	6.7		

Main statistics of the tidal (high-passed $\sigma > 0.5$ cpd) currents measured at Gibraltar's main sill (M1, M2, and M3) and eastern end (M7). The orientation of the principal axis tidal currents is measured counterclockwise from the east. The semimajor and semiminor axes of fluctuation are denoted by the standard deviation (centimeters per second) of the current along that axis. Two estimates of the spatial weights for the principal axis tidal current EOF modes are shown. One corresponds to the EOF analysis with all 12 instruments in moorings M1, M2, and M3, and the other to the analysis with only the 7 instruments from moorings M1 and M3 (given in parentheses). The variance represented by each mode, on both EOF analysis, is also indicated.

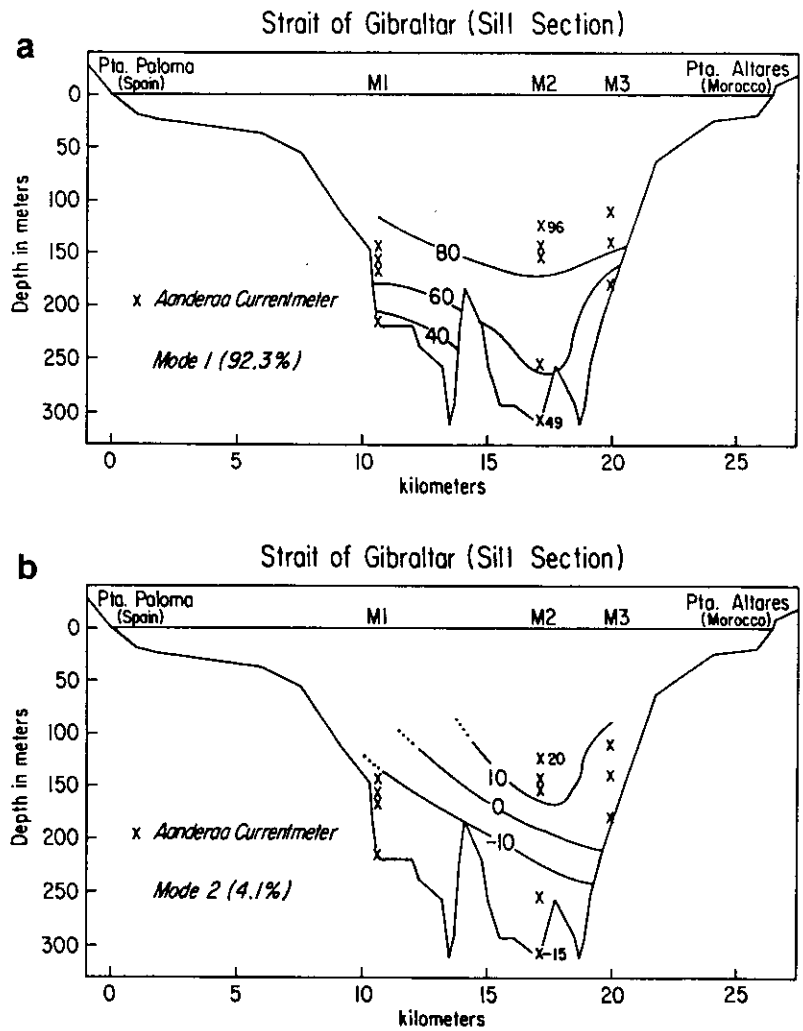

Fig. 6. Spatial structure of the first two EOF analysis modes of the principal axis tidal currents at Gibraltar's main sill section. (*a*) Structure of mode 1, explaining 92.3% of the variance at these frequencies (> 0.5 cpd). (*b*) Structure of mode 2, which explains 4.1% of the total variance contained in the tidal current field. Contours are in centimeters per second and relate to the standard deviation of the tidal current associated with each mode. The EOF analysis that beared these modes used data from all 12 instruments (crosses) on moorings M1, M2, and M3 from October to November 1985.

1985, at five depths. Low-frequency fluctuations, with periods longer than a day, are eliminated by subtracting their contribution from the raw observations of the u-east and v-north current components. The principal axis components of the high-pass time series are then computed and listed in Table 5.

Instead of comparing the pressure field to individual point measurements, it is more appropriate to find covarying modes of fluctuation for the tidal sill currents using EOFs. The covariance matrix between high-passed principal axis components of the currents from each instrument on moorings M1 and M3 (or M1, M2, and M3) is formed, and the eigenvalues and modes of that matrix are sought. Owing to the different measuring intervals that the meters in M2 have with respect to those in M1 and M3, and to the desirability of having both a long time series and a good spatial coverage, two EOF analyses were performed. The first analysis consisted of the 12 time series from all the meters in the three moorings, which have 1 month of simultaneous data. The first mode explains 92.3% of the variance and its weights, which are the rms value of the currents due to this mode at each location, are listed in Table 5 and shown in Figure 6*a*. This figure also illustrates the cross section of the sill and indicates the location of the current meters on each mooring. This mode, where tidal currents fluctuate everywhere in phase with some amplitude variation, is the closest approximation to a "barotropic" tidal current mode at the sill section. A direct average of the weights in the cross-section gives 0.71 m s^{-1}, which when multiplied by the cross-sectional area at the sill (2.951 $10^6 m^2$) gives an estimate of 2.1 Sv for the rms value of the tidal transport through the strait. The time coefficients of this first mode are shown in Figure 7*a* by the dotted line. The second EOF analysis used only the seven meters on moorings M1 and M3 for which observations were available for about 6 months. The first mode of this second EOF analyses explains 92.7% of the variance. Its spatial weights are also listed in Table 5 (in parentheses), and its time coefficients are shown in Figure 7*a* by the solid line. The inclusion of the M2 observations does not significantly alter the time evolution of the principal mode of tidal motion obtained by either of the EOFs. This is an indication of the high degree of coherence between observed tidal currents across the section. Vector cross spectra between any pair of current observations at the sill section give a total correlation coefficient greater than 0.97 for the semidiurnal band.

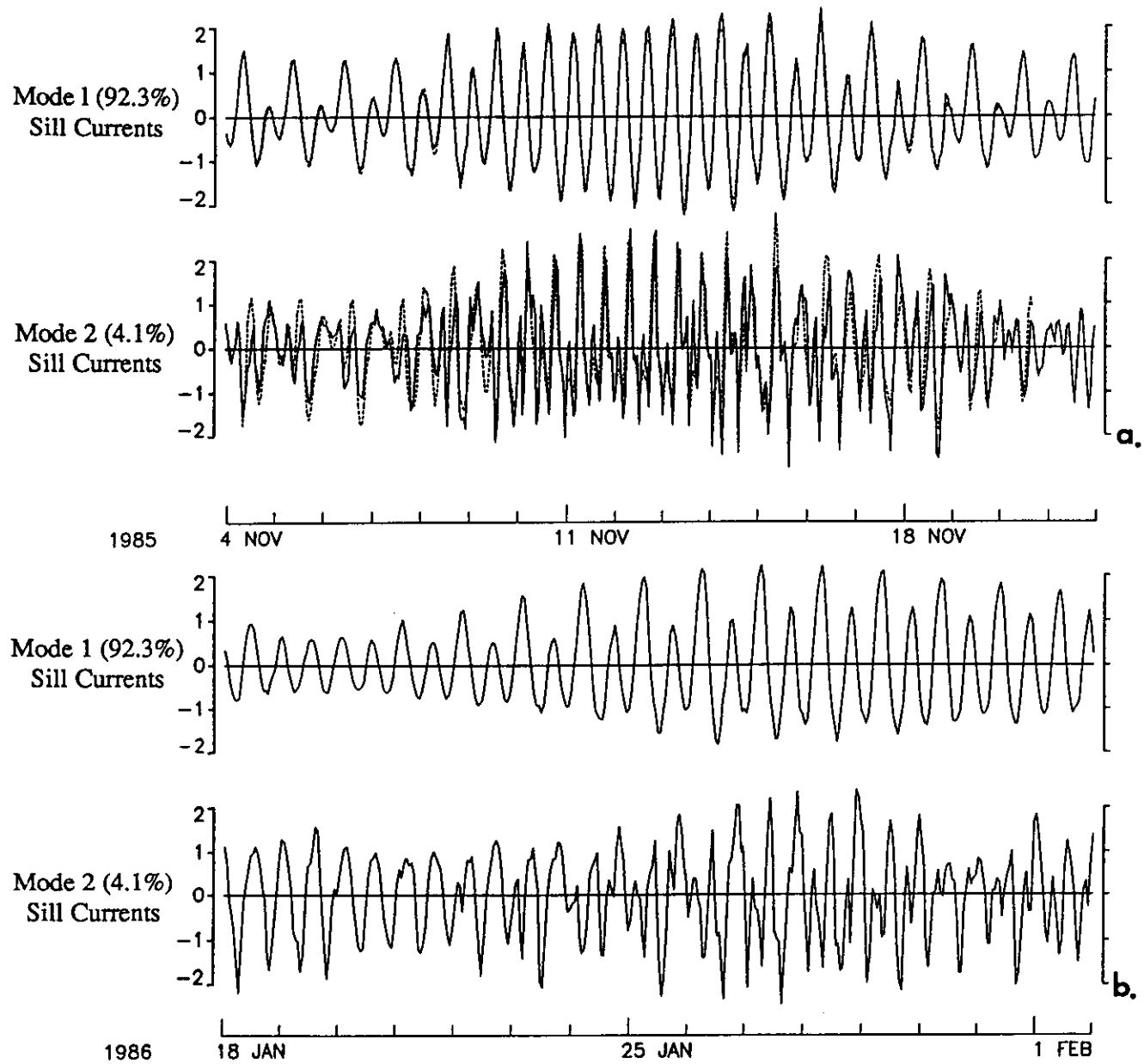

Fig. 7. Time coefficients of the first two EOF analysis modes of the principal axis tidal currents shown in Figure 6, chosen to be dimensionless. (*a*) The dotted line is obtained by considering all 12 measurements available from the three moorings at the sill section covering a month of observations (October to November 1985). The continuous line relates to the result when only the seven instruments from moorings M1 and M3 are considered covering a period of 6 months (October 1985 to April 1986). Only a 15-day period (November 4–22, 1985) is shown for clarity. (*b*) Time coefficients of modes 1 and 2 of the tidal currents based on data only from M1 and M3. The 15-day period between January 18 and February 2, 1986 is shown so direct comparison with other figures in the paper is possible.

The second mode of the EOF analyses accounts for 4.1 or 4.9% of the variance, depending on the number of measurements used. Its spatial structure (Figure 6*b* and Table 5) resembles a first baroclinic mode with a node coinciding with the approximate mean location of the interface between Atlantic and Mediterranean waters. The time evolution of this mode is quite erratic (Figures 7*a* and 7*b*), and the variation in weights, depending on which EOF is used, indicates that the available data is not adequate for completely resolving its structure or time behavior. However, this second mode is the manifestation of the internal tide at the sill section, and the EOF analysis has provided a quantitative estimate of its contribution to the currents sensed at the section.

The mode illustrated in Figure 6*a* is taken to represent the spatial structure of the main tidal current signal at the sill and its time behavior as that obtained from the longer pressure EOF (mode 1, solid line, Figure 7). This current mode will be used, in conjunction with the pressure field modes previously described, to verify the simple dynamical balances assumed for the tides in the strait. This mode of the currents at the sill has an M_2 phase of 140.2° and an amplitude of 1.24. The phase difference of near 90° between the main current and pressure modes at the sill supports the idea of a standing wave behavior for the M_2 constituent in the strait. It is interesting to notice that in the strait, ebb current (toward the Atlantic) precedes high water, as if a node in elevation for each of the principal semidiurnal constituents were present

inside the Mediterranean. The 90° phase relation is also indicative of a nearly zero tidal energy flux through the strait.

To investigate the along-strait momentum balance, the along-strait pressure gradient is estimated by fitting a plane of the form: $P = a_o + a_1 x + a_2 y$ (where P is pressure, x and y the east and north Cartesian coordinates of the stations location, and a_o, a_1, and a_2 are fitting coefficients), to the weights of mode 1 corresponding to the four pressure stations located over the sill area, i.e., SN, DN, DS and SS. The results give $a_1 = \partial P/\partial x = -0.1067\ 10^{-2}$ mbar m^{-1} and $a_2 = \partial P/\partial y = -0.9251\ 10^{-4}$ mbar^{-1}, so the local maximum pressure gradient has magnitude of $1.071\ 10^{-3}$ mbar^{-1} and is oriented -175° with respect to east. If this is taken as representative of the local along strait pressure gradient, then the term $-\rho^{-1}\ \partial P/\partial x_o$ (where ρ = 1028 kg m^{-3} and x_o is the along-strait coordinate) has an rms value of $10.42\ 10^{-5}$ m s^{-2}, and when multiplied by the mode 1 time coefficients (Figure 5) gives a time series for this term. To estimate $\partial u/\partial t$, the mean value of the mode 1 sill currents (71.32 cm s^{-1}) (Figure 6*a*), is multiplied by its time coefficients, and a time derivative of the resulting series is calculated using splines [*Forsythe et al.*, 1977]. The comparison between the two terms (Figure 8*a*) is remarkable; the correlation coefficient between the two series is 0.94. Considering that the current and pressure fields being compared are independent measurements, the agreement underlines the quality of both sets of observations.

The residual between the two terms (bottom plot, Figure 8*a*) is noisy and its variance is about an order of magnitude smaller than any of the two terms considered. It is interesting to note that friction seems to play a minor role in the balance, if present it should be at least an order of magnitude smaller than either of the other two terms, since its contribution would have to be extracted from the residual. However a friction term in phase and correlated to the current u is not well supported by these observations. Still, if it is assumed that at least the variance contained in the residual, with an rms of $3.5\ 10^{-5}$m s^{-2}, could be explained by a linear frictional term of the form λu, then $\lambda \simeq 5.\ 10^{-5}$s^{-1}, since the rms of the tidal u is 0.71 m s^{-1}. This λ implies an e-folding decay time scale of about half of the semidiurnal tidal period (5.6 hours),

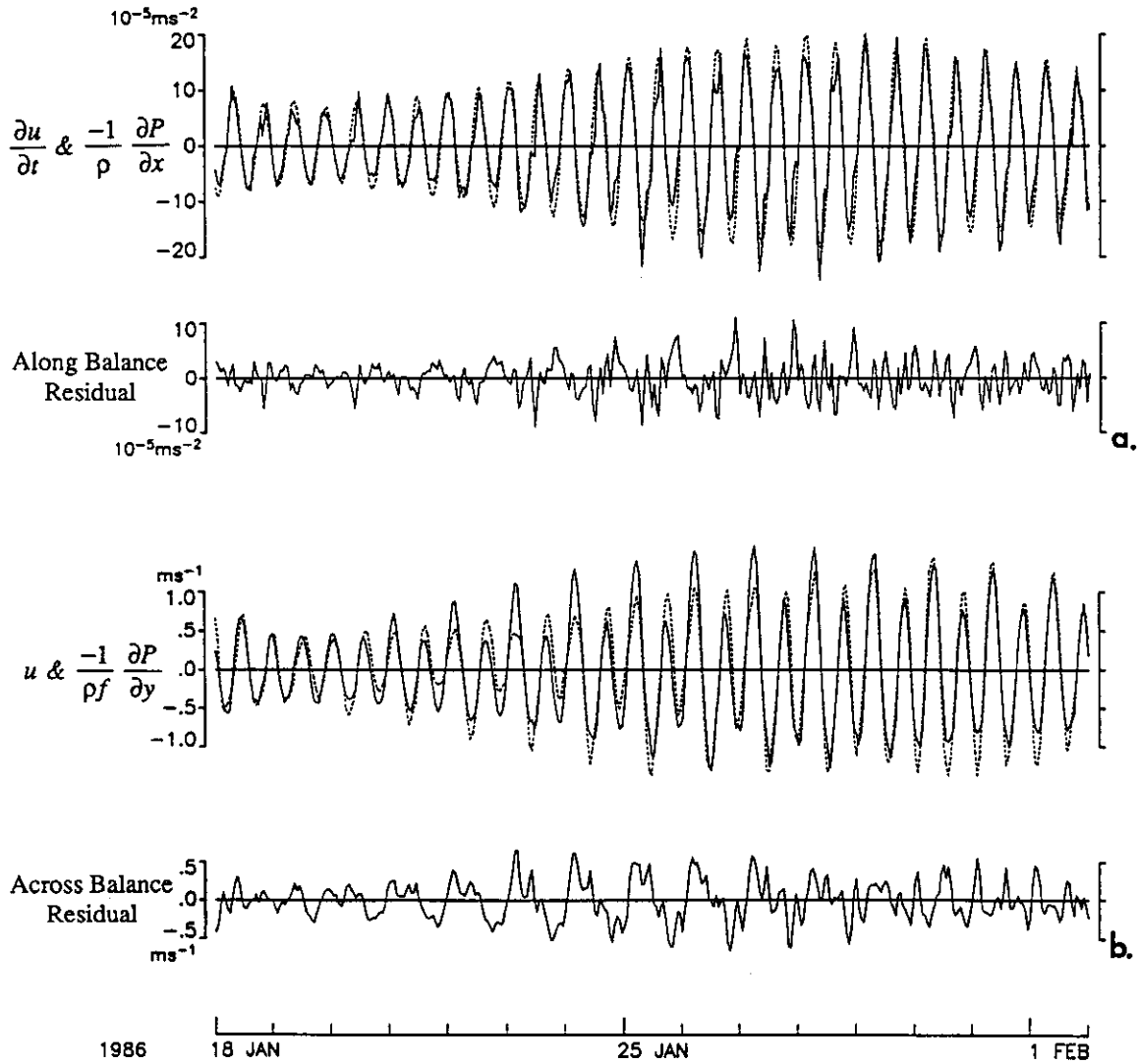

Fig. 8. Series of the principal terms in the along- and across-strait tidal momentum balance at the main sill. (*a*) Principal along-strait momentum balance terms. The top plot shows $\partial u/\partial t$ (solid line) and $-\rho^{-1}\partial P/\partial x$ (dotted line). The bottom plot shows the difference between the two terms plotted above. (*b*) Principal terms in the across-strait tidal momentum balance at Gibraltar's main sill. The top plot shows the observed tidal current u (solid line) and the across-strait pressure gradient $-(\rho f)^{-1}\partial P/\partial y$ (dotted line). The bottom time series (across balance residual) is the difference of the two terms plotted above.

a result in agreement with that obtained for the subinertial flows through the strait by *Candela et al.* [1989]. The value of $\lambda = 5.\ 10^{-5}s^{-1}$ as obtained above, implies having a perfect correlation coefficient ($r = -1.$) between u and the along-strait momentum balance residual. The available series give $r = -0.36$, so the data only support a value of $\lambda = 1.84\ 10^{-5}s^{-1}$ (15.4 hours). This last value agrees well with the accepted relation of $\lambda = CU/H$, where C is a dimensionless drag coefficient ($\sim 3 \times 10^{-3}$), U is an rms current velocity (0.71 m s^{-1}), and H is the hydraulic depth (cross-sectional area/width ~ 120 m), which gives $\lambda = 1.75\ 10^{-5}s^{-1}$. Even though the data points to this smaller value for the linear friction coefficient, it is believed that this represents a lower limit to the possible magnitude of the effects of friction in the strait. The noise content in the along-strait momentum balance residual does not permit a proper evaluation of the effects of friction, but based on the available data, λ should have a value between 1.8 and $5 \times 10^{-5}s^{-1}$ in the strait. If friction is parameterized instead by a quadratic relation, the value for the dimensionless drag coefficient should then fall between 0.003 and 0.008.

To verify if the simple along-strait balance found at the sill is also present at the eastern end, the first mode of pressure is compared with current measurements from mooring M7. For the eastern end, the along-strait pressure gradient implied by mode 1 (Figure 4*a*) is calculated by a plane fit to the weights from stations CE, AL, DP5 and TA. The magnitude of this gradient is about half of that found at the sill, with a value of $4.816\ 10^{-4}$ mbar m^{-1}, oriented -157° with respect to east. This gives an rms value for the term $-\rho^{-1}\partial P/\partial x_o$ at the eastern end of $4.685\ 10^{-5}$m s^{-2}. Mooring M7 has only two instruments, i.e., M7-54 m and M7-193 m, and from the previous discussion of Figure 2*b*, it is observed that the upper layer currents (M7-54 m) have a weak and erratic tidal signal. In this case a simple balance between local acceleration and the pressure gradient is not expected and indeed it is not observed for the upper layer. The lower layer (M7-193 m), however, does comply with this simple along-strait momentum balance (Figure 9). It is encouraging to find such a good agreement (correlation coefficient 0.91), even when comparing the pressure field with the local acceleration term deduced from the currents measured at only one point in the lower layer. The correlation between the residual in Figure 9 and the u in the lower layer (M7-193 m) is only -0.28, but the slope value of the regression surprisingly gives again $\lambda = 1.85\ 10^{-5}s^{-1}$, confirming the lower limit estimate for the effects of friction obtained at the sill previously.

The across-strait momentum balance is verified by comparing mode 2 of the pressure field (Figure 4*b*) with the first mode of currents at the sill (Figure 6*a*). Again fitting a plane to the four sill stations for mode 2 (Figure 4*b*), a north-south pressure gradient of $-0.6297\ 10^{-3}$ mbar m^{-1} is obtained. This gives an rms value for the term $-(\rho f)^{-1}\ \partial P/\partial y$ (where $f = 8.5115\ 10^{-5}s^{-1}$ is the Coriolis parameter) of 0.7197 m s^{-1}, which when multiplied by the time coefficients of mode 2 (bottom plot, Figure 5) gives a time series for this term. To see how geostrophic the tidal flow is at the sill section, $-(\rho f)^{-1}\ \partial P/\partial y$ is compared with the first mode of currents at the sill. The agreement is reasonably good (Figure 8*b*), the correlation coefficient is 0.92, but there are appreciable discrepancies mainly in amplitude.

In contrast to $\partial P/\partial x_o$, $\partial P/\partial y$ is expected to vary considerably with depth. Due to the correction performed on the deep sill pressure measurements, $\partial P/\partial y$ is measuring the across-strait pressure gradient at the surface and so relates to the surface currents. On the other hand, the mode 1 current (Figure 6*a*) used in Figure 8*b* refers to a "barotropic" current. In principle, the residual of the across-strait balance (Figure 8*b*) should be related to the baroclinic current. A good correlation could be expected between this residual and mode 2 of the sill currents (Figure 7*b*, bottom plot), which has an obvious baroclinic structure, but the data do not show it. Unfortunately, there are no current measurements available near the surface, and the current modal decomposition used is based mostly on observations from the lower layer. The internal

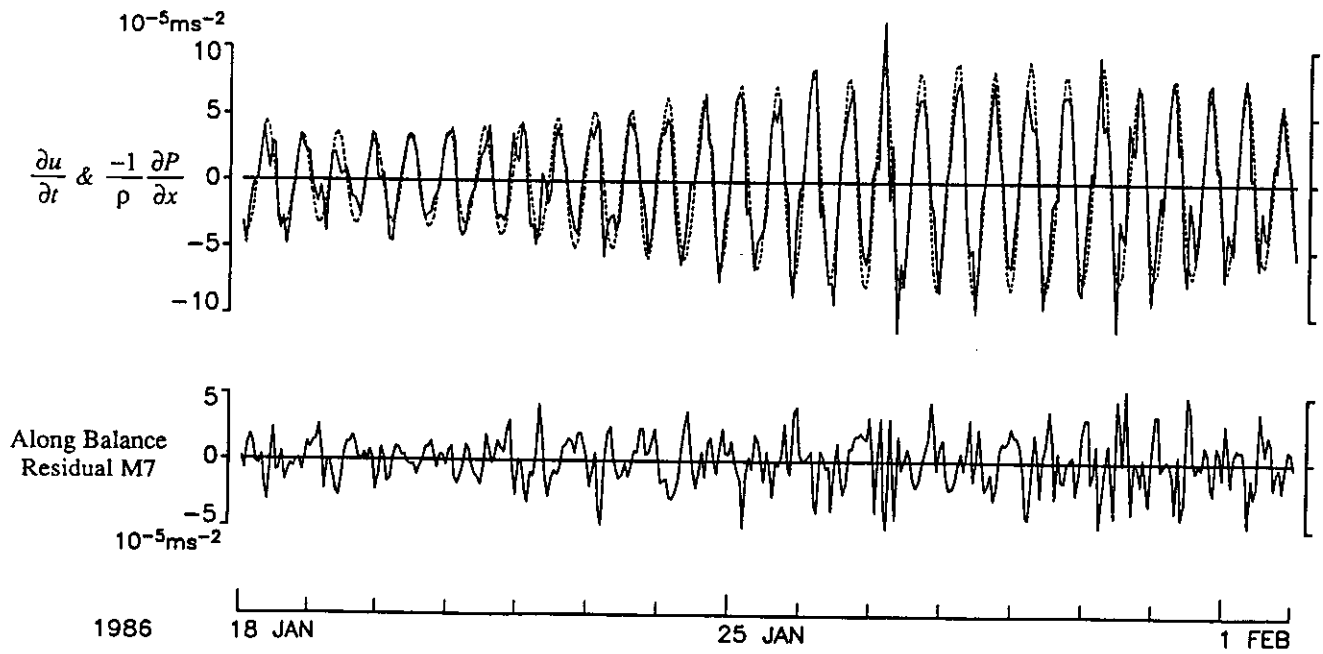

Fig. 9. Series of the principal terms in the along-strait tidal momentum balance for the lower layer at the eastern end of the strait, i.e., Algeciras-Ceuta section. The top plot shows $\partial u/\partial t$ (solid line) computed from the principal axis tidal current observed at M7-193 m and $-\rho^{-1}\partial P/\partial x$ (dotted line) obtained from the pressure data around the section. The bottom curve gives the difference of the two terms plotted above. Note the difference in vertical scales when comparing with Figure 8*a*.

tide at the sill would have to be very stable and have appropriate vertical symmetry for the second mode (Figure 6*b*) to also account for the upper layer baroclinic variability. Another consideration is that $\partial P/\partial y$ is not likely constant across the strait. It is a well known fact, usually pointed out to mariners in charts of the strait, that tidal currents inshore turn earlier than offshore. Thus at given times within a tidal cycle, the shape of $\partial P/\partial y$ should differ substantially from a straight line as is implicit in the plane fit used to evaluate $\partial P/\partial y$. Maybe most of the observed residual could be explained by this discrepancy alone.

At the eastern end the tidal currents in the upper layer do not seem to agree with a geostrophic balance. This is at first surprising when at subinertial frequencies it is observed that the pressure difference between Ceuta and Algeciras (or Gibraltar) is in excellent agreement with a geostrophic across-strait balance. In fact, it is very reasonable to take the across-strait pressure difference as representative of the subinertial fluctuations of the upper layer inflow into the Mediterranean [*Kinder and Bryden*, 1987]. At tidal frequencies, though, the relatively small magnitude of the upper layer tidal current at M7-54 m, coupled to the nearly identical amplitude and phase for the tidal pressure signal observed at the north (AL) and south (CE) shores, makes the corroboration of a tidal geostrophic balance very dependent on small errors in the data. A further consideration is that across strait pressure differences relate to an average current across the strait, along a line joining the two pressure instruments at either side. If there is across-strait variability of the along-strait tidal current, the pressure difference and the currents measured at a point in between need not be well correlated.

It is interesting to observe that even in a place like Gibraltar, with complicated topography and strong flows ($O(0.5\ \mathrm{m\ s^{-1}})$) at lower frequencies (< 0.5 cpd), the tides in the strait present simple dynamical balances which are the same as those governing the tide in the deep ocean. The best wave model for the deep ocean tides is Kelvin waves [*Hendershott*, 1973]. A Kelvin wave traveling along a boundary has a geostrophic balance in the across-boundary direction, while in the along-boundary direction the acceleration of the flow is balanced by the pressure gradient and some dissipation or friction term. In a strait, these same balances seem to dominate the dynamics of the barotropic tide. This tidal behavior has been verified in other straits, [e.g., *Garrett and Petrie*, 1981; *Godin et al.*, 1981]. For example, in the strait of Juan de Fuca, south of Vancouver Island on the west coast of North America [*Godin et al.*, 1981], the M_2 cotidal chart has a configuration completely reversed from that in the Strait of Gibraltar. There, cotidal lines are somewhat perpendicular to the axis of the strait, increasing in magnitude towards the interior. Corange lines are also perpendicular to the axis in the western part of the strait but become parallel to the axis towards the eastern end increasing in magnitude southward. Still, tidal currents and sea level observations comply with the dynamic balances of a Kelvin wave. Actually this cotidal pattern can be shown to be the manifestation of a local degenerated (virtual) amphidromic system, whose node has been forced to fall outside the channel due to the effects of friction. Interestingly, a linear friction coefficient of $\lambda = 4\ 10^{-5}\mathrm{s}^{-1}$ is required to best fit the M_2 tidal observations in Juan de Fuca, which is within the range of values deduced from the Gibraltar data discussed previously.

Apart from the complicated tidal behavior observed in the surface at the eastern end, the following interpretation of the observed tides in the Strait of Gibraltar can be given as a conclusion to this section: The strait has to match two very different tidal regimes (Atlantic and Mediterranean), mainly by an along-strait amplitude gradient. Since this amplitude gradient has very little cross-strait structure, it cannot accommodate a geostrophically balanced tidal flow. As a consequence, a gradient in phase is needed across to produce the pressure difference between the north and south shores to balance the Coriolis acceleration associated with the tidal currents.

4. TIDAL CURRENTS IN THE STRAIT

This section gives a description of the tidal currents which are coherent with the vertical tide as deduced by the use of admittance calculations [*Godin*, 1978]. A brief review of admittance estimates in current series is included in Appendix B.

As an end result of these admittance calculations, current ellipses are obtained for the main tidal constituents within the diurnal and semidiurnal bands (O_1, Q_1, P_1, and K_1 for the diurnal, and N_2, M_2, S_2, and K_2 for the semidiurnal), for the higher-frequency bands it is still necessary to rely on the direct harmonic analysis estimates. Results of these analyses for all of the sites where current meters were deployed are summarized in Table 6, for the two principal components of the semidiurnal band (S_2 and M_2). The pressure record at DN was used as input; similar results are obtained if the Ceuta pressure or the Cadiz sea level are used as inputs. Due to the uncertainties in the determination of the diurnal tidal constituents, they are not discussed in detail here.

By extracting that part of the tidal streams which is coherent with the vertical tide, that portion of the currents which is "predictable" is obtained. This predictable part represents periodic currents where the ebb and flood are collinear and of the same amplitude, always rotate in the same sense, and maintain a constant phase. The remainder energy found in each tidal band is made up of all the different distortions that the tidal ellipse might have due to the presence of a varying internal tide, interactions with topography and nonlinearities. Table 7 indicates the percentage of "predictable" tidal current, in the diurnal and semidiurnal bands, at each available measurement location.

Tidal Transports

There is a definite structure to the ellipse parameters given in Table 6: At the sill, and west of the sill, the amplitude of the ellipse decreases with depth, in the sense expected given the influence of friction. East of the sill the amplitude of the semidiurnal currents increases with depth, being larger in the lower layer than in the upper layer. Time-averaged currents show a different behavior: in the upper layer the mean currents increase eastward of the sill, and the same is true for subinertial currents (Table 3). This increased amplitude observed for the mean and low-frequency currents is consistent with the smaller sectional area of the mean upper layer at the eastern end (between Algeciras and Ceuta), compared with the sill [*Lacombe and Richez*, 1982].

To understand the behavior of tidal currents, it is helpful to compare transports in each of the two layers at the sill and at the eastern section. Since transports are not directly observed, they must be estimated from point measurements of velocity. At the sill there are no direct current measurements at depths shallower than 100 m, but the lower layer is reasonably well covered. In order to obtain estimates of the lower as well as the upper cross-sectionally integrated currents, it was chosen to use the EOF decomposition of Figure 6, superposing the contribution of modes 1 and 2 for each layer. Mode 1 is the same for both layers, but mode 2 has differing sign depending on the layer. Since nonlinear

TABLE 6. Principal Semidiurnal Tidal Ellipses (M_2 and S_2) for the Current Meter Observations Listed in Table 2

Station	Depth of Instrument, m	M_2				S_2			
		M, cm s^{-1}	m, cm s^{-1}	θ, deg	g, deg	M, cm s^{-1}	m, cm s^{-1}	θ, deg	g, deg
M1	143	85	-5	353	133	31	-2	353	159
	156	81	-6	340	133	29	-2	340	159
	167	77	-6	351	132	28	-2	351	158
	215	44	-2	344	124	16	-1	344	150
M2	90	115	2	3	141	41	1	3	168
	112	111	4	8	155	40	1	8	181
	123	112	-3	11	154	40	-1	11	180
	135	118	-7	17	156	42	-3	17	182
	143	106	-6	14	154	38	-2	14	180
	153	113	-9	17	153	41	-3	17	179
	181	99	-14	20	132	36	-5	20	158
	233?	73	0	26	124	26	0	26	150
	254	79	1	30	133	28	0	30	159
	299?	53	0	40	102	19	0	40	128
	306	58	3	43	133	21	1	43	159
M3	102?	107	-3	6	124	39	-1	6	150
	110	115	-3	9	146	41	-1	9	172
	127	101	-6	12	144	36	-2	12	170
	140	104	-5	12	148	37	-2	12	174
	172	49	-2	18	146	18	-1	18	172
	180	66	-3	12	145	24	-1	12	171
M4	67	50	1	16	135	18	0	16	161
	340	26	-6	33	114	9	-2	33	140
M7	54	21	-6	20	208	8	-2	20	234
	193	37	2	26	139	13	1	26	165
M8	30	67	3	15	156	24	1	15	182
M9	58	49	2	13	189	18	1	13	215
	159	61	1	17	124	22	1	17	150
F1	204	16	-4	11	124	6	-1	11	150
	260	14	-2	11	120	5	-1	11	146
	320	22	0	23	170	8	0	23	196
	380	12	0	59	149	4	0	59	175
F2	220	19	-1	27	163	7	0	27	189
	280	57	0	27	164	20	0	27	190
	320	32	-3	16	131	12	-1	16	157
F3	63	111	3	12	143	40	1	12	169
	126	115	-5	16	145	41	-2	16	171
	165	77	-6	29	125	28	-2	29	151
	225	81	0	40	130	29	0	40	157
F4	60	49	-2	24	182	18	-1	24	208
	120	37	-1	19	135	13	0	19	161

Admittance calculations with Deep North pressure station predictions have been used to separate K_2 from S_2. M is the semimajor axis (centimeters per second). The sign of the semiminor axis (m, in centimeters per second) indicates the sense of rotation of the tidal current (positive counterclockwise). Orientation (θ) and phase (g) correspond to flood current (into the Mediterranean). The orientation is trigonometric measured counterclockwise from the east. Phases, which indicate the time of occurrence of maximum flood current, are in degrees with respect to GMT. Instruments marked with a question mark are suspected of timing errors. Information for the two deployment times of moorings M2 and M3 has been merged into one column, according to depth of instrument.

flow interactions are expected, transport calculations require the inclusion of the subinertial variability on the current estimates used. This is incorporated in a similar way as the tidal part, by adding the contributions of modes 1 and 2 of the subinertial currents described by *Candela et al.* [1989, Figures 2, 3, and 4]. In this way, smooth estimates of the upper and lower layer total fluctuating currents are obtained, which in addition to including the barotropic effect (modes 1, tidal and subinertial), incorporates the main baroclinic variability in each layer (modes 2, tidal and subinertial). At the eastern end (Ceuta-Algeciras section) there is only one direct current measurement in each layer. Therefore, in lack of a better coverage, the upper layer currents are taken as the demeaned principal axis currents measured at M7-54 m, and the lower layer currents as those measured at M7-193 m. It could be argued that these represent overestimates of the actual cross-sectionally integrated currents, since the meters are located in a central position in each layer. However, if so, this overestimation does not affect the qualitative results of the model discussed later.

The cross-sectional area of the upper and lower layers are functions of the interface depth fluctuations. It is always ambiguous to determine which single parameter value is to be identified with the interface. Here the 37.0‰ isoline is taken as representing the interface between Atlantic and Mediterranean waters. Although this arbitrary definition of the interface must imply an unknown bias on the mean transports calculated, it is as good a definition as any other value of salinity or temperature within the interface, to account for the fluctuations of the depth of the interface or the cross-sectional areas variability deduced from it. The depth of the

TABLE 7. Tidal Current Coherent With the Vertical Tide

Station	Depth of Instrument, m	Diurnal Band: Semimajor Axis, cm s^{-1} Total	Diurnal Band: Semimajor Axis, cm s^{-1} Residual	Diurnal Band: % of Coherent Current	Semidiurnal Band: Semimajor Axis, cm s^{-1} Total	Semidiurnal Band: Semimajor Axis, cm s^{-1} Residual	Semidiurnal Band: % of Coherent Current
M1	143	34.9	14.8	57.6	91.8	16.4	82.1
	156	32.4	13.9	57.1	86.2	12.6	85.4
	167	30.7	13.3	56.7	82.6	13.0	84.3
	215	16.3	8.4	48.5	47.7	9.8	79.5
M2	90	51.4	23.8	53.7	120.7	31.3	74.1
	112	49.2	26.4	46.3	117.6	22.6	80.8
	123	49.5	24.3	50.9	124.1	14.7	88.2
	135	45.5	17.7	61.1	123.2	28.9	76.5
	143	48.6	22.5	53.7	118.4	19.1	83.9
	153	53.0	22.7	57.2	125.6	21.3	83.0
	181	45.1	17.8	60.5	99.6	18.0	81.9
	233	32.8	13.4	59.1	77.3	15.1	80.5
	254	35.0	12.6	64.0	87.8	14.4	83.6
	299	22.2	11.5	48.2	56.8	11.0	80.6
	306	28.7	11.2	61.0	64.6	12.1	81.3
M3	102	43.7	16.6	62.0	105.1	15.4	85.3
	110	47.6	19.7	41.4	122.9	15.4	87.5
	127	39.5	16.1	59.2	90.4	11.1	87.7
	140	40.3	16.4	59.3	110.8	16.7	84.9
	172	20.7	10.6	48.8	50.7	8.9	82.4
	180	26.2	13.5	48.5	71.5	16.3	77.2
M4	67	17.1	8.4	50.9	46.5	5.3	88.6
	340	19.0	8.6	54.7	28.3	6.8	76.0
M7	54	32.1	17.4	45.8	31.0	21.1	31.9
	193	15.5	8.6	44.5	39.1	7.9	79.8
M8	30	27.3	13.6	50.2	70.4	10.3	85.4
M9	58	28.1	14.2	49.5	52.5	16.7	68.2
	159	22.9	13.1	42.8	65.1	14.0	78.5
F1	204	5.2	3.7	28.8	15.4	3.8	75.3
	260	6.6	5.1	22.7	15.9	8.2	48.4
	320	6.7	5.7	14.9	21.6	6.1	71.8
	380	3.2	2.8	12.5	11.9	3.2	73.1
F2	220	13.9	8.6	38.1	22.2	6.8	69.4
	280	48.1	28.0	41.8	60.6	18.3	69.8
	320	14.1	7.5	46.8	33.3	6.2	81.4
F3	63	43.6	27.7	36.5	112.3	11.9	89.4
	126	48.9	33.7	31.1	117.1	22.3	81.0
	165	26.1	19.0	27.2	79.1	15.6	80.3
	225	26.7	17.9	33.0	81.4	13.5	83.4
F4	60	30.7	20.6	32.9	48.2	14.2	70.5
	120	12.3	8.3	32.5	35.4	6.1	82.8

Percentage ratio of the semimajor axis of the diurnal and semidiurnal currents coherent with the pressure measurements, to that of the original current observations (total), i.e., ({1.-[residual/total]} * 100.), where residual = total-coherent. The coherent currents are predictions based on the main diurnal and semidiurnal tidal constituents deduced from admittance calculations with DN pressure station. The semimajor axis are obtained by vector power spectra using a frequency resolution of $\Delta\sigma$ = 1 cpd.

37.0‰ isoline is linearly interpolated for, at every hour, using the depth and salinity records from two simultaneous instruments at differing depth on a mooring. Since at times the isoline defining the interface might be found shallower than the upper instrument or deeper than the deepest meter, fixed salinity values of 36.2‰ (characteristic of Atlantic water) at 10 m and 38.4‰ (characteristic of Mediterranean water) at 300 m, were specified. At the sill the interface depth records calculated on M1 and M3 are average, and the resulting series is taken as representing the fluctuations of the interface at the sill, while at the eastern end the series obtained on M7 is used. Time series of upper and lower layer cross-sectional areas, at the sill and eastern end, are then calculated using a numerical algorithm based on the strait's depth data at each section.

Results are illustrated in the upper two Figures 10*a* and 10*b*. The behavior of tidal currents noted earlier is even more apparent in the transports: it is clear that the largest transport at tidal frequencies occur in the upper layer at the sill, and in the lower layer at the eastern section, and thus the major component of the tidal transport shifts from the upper to the lower layer east of the sill. It is interesting to note that even though the 5-month-long time series of currents used in these computations had the time average removed, the transports in each layer have a significant mean, amounting to 0.21 Sv flowing toward the Mediterranean in the upper layer and 0.17 Sv flowing toward the Atlantic in the lower layer at the sill. These mean transports which result from mean correlations between fluctuating currents and interface depths at subinertial and tidal frequencies, amount to a significant fraction of the mean exchange through the strait, estimated to be of the order of 1 Sv in each layer [*Lacombe and Richez*, 1982]. Their

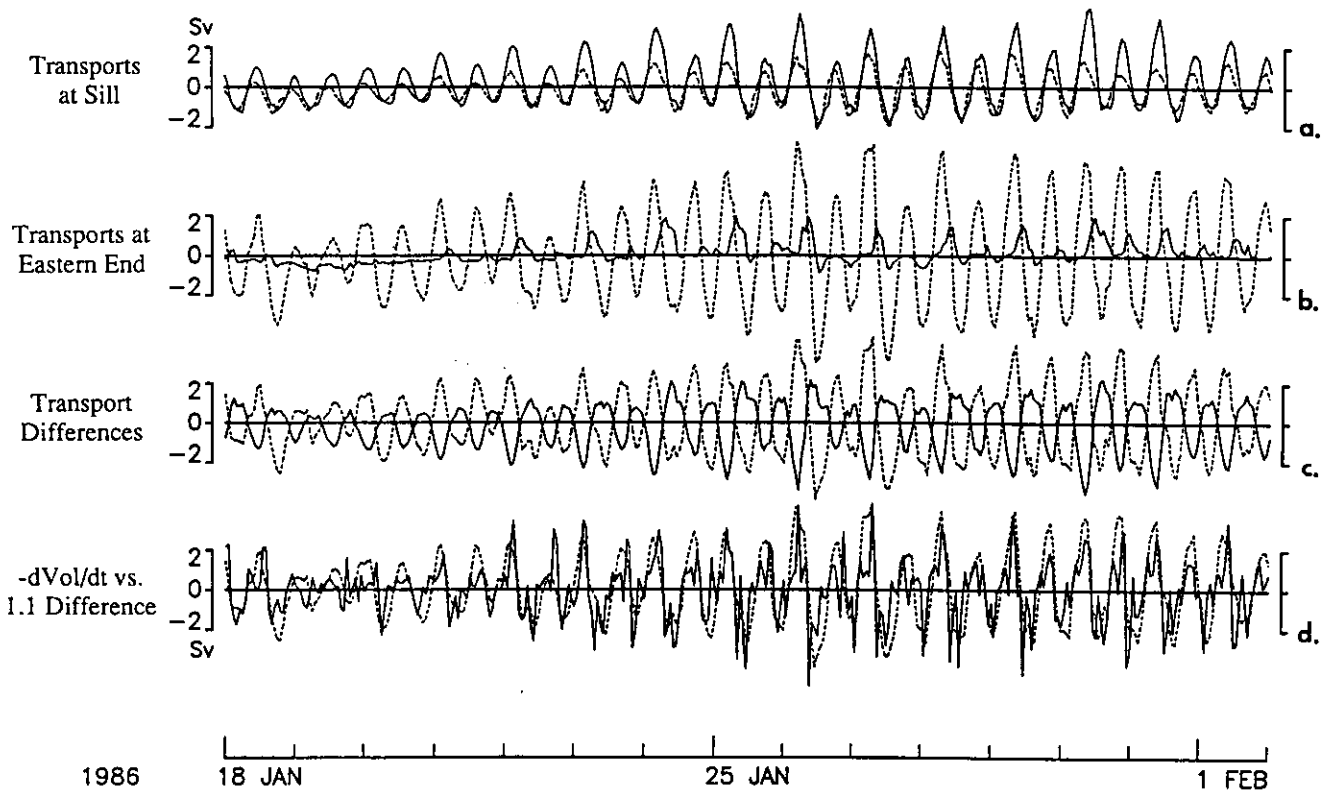

Fig. 10. Tidal and subinertial transport calculations through the strait: (*a*) upper (TSU, solid line) and lower (TSL, dotted line) layer transports at the sill, (*b*) upper (TEU, solid line) and lower (TEL, dotted line) layer transport at the eastern end (Ceuta-Algeciras section), (*c*) upper (TEU-TSU, solid line) and lower (TEL-TSL, dashed line) layer transport difference between eastern and sill sections, and (*d*) terms in the mass conservation equation for the lower layer, time rate fluctuation of volume of the lower layer ($-d\mathrm{Vol}/dt$), solid line) and transport difference between east and sill sections (same as in Figure 10*c*, dashed). All transports are in sverdrups (1 Sv = $10^6 \mathrm{m}^3\mathrm{s}^{-1}$).

evaluation is not significantly affected by the lack of shallow current measurements, since the region where current and interface fluctuations interact, which is where these rectified mean transports are generated, is reasonably well covered by the available current data. Only 10% of these rectified transports is related to subinertial motions, while the tides account for the rest. The difference between the mean transports due to the interactions, 0.04 Sv, is small enough and subject to uncertainties, but it is noteworthy that it is of the right sign and magnitude to explain the mass loss to evaporation in the Mediterranean.

Differences between the transport into and out of each layer are illustrated in Figure 10*c*. Given that the free surface of the upper layer changes only very little, compared with displacements of the interface, the two time series illustrated in this frame are expected to fluctuate in opposition, so as to conserve the total mass in the combined upper and lower layers. The difference between flow in and out of each volume can exceed 2 Sv and must be balanced, by continuity, by changes in the volume of each layer: for example, the time rate of change of the volume of the lower layer, $-d\mathrm{Vol}/dt$, must equal the difference in transport into and out of the layer. Time series of the interface depth at either end of the volume are available, and the time rate of change of the volume is crudely estimated assuming a linear interface between these two extremities. The comparison is illustrated in Figure 10*d*. It is clear that there is a close correspondence between the rate of change of the volume and the transport difference in the lower layer, the correlation between the two records is 0.58, significantly different from zero at the 99% confidence level.

These simple mass balance arguments illustrate how the tidal frequency transport is transferred from the Atlantic waters into the Mediterranean: in this regard, the interface can be viewed as a membrane which separates the two masses. When the tide floods into the Mediterranean across the sill, the interface bulges down just east of the sill and forces an equivalent flux of Mediterranean water (i.e., lower layer) out of the strait at the eastern boundary. The reverse process takes place at ebb tide. This mechanism accounts for the tidal signal reduction in the upper layer currents sensed at the eastern end (M7-54 m), with respect to those measured elsewhere in the strait.

A further calculation was performed to find which interface salinity value and weights for the upper and lower measured currents at the eastern end simultaneously gave the best transport estimates. The criterion used was to minimize the variance of the sum of the transport difference in the two layers, i.e., the two curves plotted in Figure 10*c*. Based on the available data, the best estimates were obtained when a salinity value of 37.2‰ defined the interface, the upper layer currents at M7 (M7-54 m) were weighted by 0.35 and those in the lower layer (M7-193 m) by 0.76. The results though were qualitatively the same and do not differ much in magnitude from those of Figure 10. Furthermore, about the same values for the mean rectified upper and lower layer transports are obtained at the sill, giving again a net difference of 0.04 Sv into the Mediterranean.

Armi and Farmer [1988] documented a behavior of the interface similar to that just described, but occurring to the west of the sill in the region north of Tangier. However, on this side of the

sill the situation is inverted with respect to the east side in the sense that it is the lower layer current to the west where the tidal signal proportion diminishes (see Table 3 data for F1, F2, and M4). They also mention in the conclusions [*Armi and Farmer*, 1988, pp. 33–34] that the Atlantic layer, east of the sill, acts as a fluctuating reservoir of water, in the manner that Figure 10 depicts.

Vertical Profile of the M_2 Current at the Sill

A basic description of the M_2 ellipse at the sill section is now given. This description can be considered as representative of the statistically and dynamically stable mean tidal current observed, which has the practical aspect of being that part of the current which is "predictable." Furthermore, at the sill section this part represents more than 80% of the observed semidiurnal tidal current at any given time (Table 7).

Figures 11 and 12 show the ellipse parameters for the M_2 current at the sill section; these are the semimajor axis M, the Greenwich phase g (i.e., time of occurrence of the maximum current), the orientation θ of the semimajor axis with respect to the east, and the semiminor axis m. All are deduced from admittance calculations with Deep North station. For the meters in M1 and M3, there are long (> 3000 hours) time series available, and both admittance calculations and direct harmonic analysis give very similar results. Mostly results from the analysis done on records from the first deployment (October 1985 to May 1986) are used in drawing the figures, since some starting time errors are suspected on some of the meters, at 233 m and 299 m on M2 and at 102 m on M3, form the second deployment period (May 1986 to October 1986). Results from the analysis of the short-lived F3 mooring at the sill corroborate the values shown in the two figures.

Figure 11 shows contours of the semimajor axis for M_2 (solid line). Maximum currents of 115 cm s^{-1} are observed toward the upper southern portion, diminishing to values of ~ 55 cm s^{-1} toward the bottom due to frictional effects. Unfortunately there are no shallow (< 100 m) measurements, and it is possible that larger currents might be found there near the center of the section. However, geostrophically deduced tidal currents from pressure difference between SS and SN (April–August 1986) give mean across-strait M_2 amplitude of only 92 cm s^{-1}. Still, with this

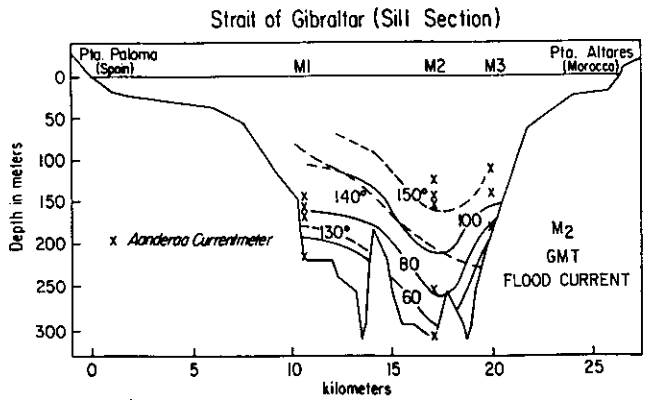

Fig. 11. Contours of the semimajor axis (centimeters per second, solid line) and phase lag (degrees with respect to GMT) of the current ellipse contributed by the principal lunar semidiurnal constituent M_2 at Gibraltar's main sill. The phases given indicate the time of occurrence of maximum M_2 flood current, i.e., into the Mediterranean. M_2 frequency is 28.98° h^{-1}

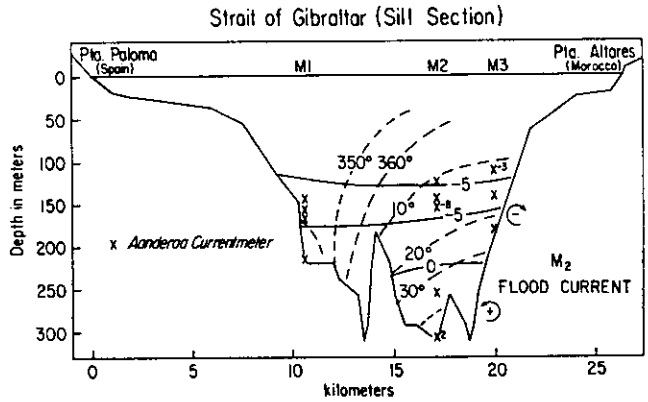

Fig. 12. Contours of the semiminor axis (centimeters per second, solid line) and orientation (trigonometric degrees measured counterclockwise from the east, dashed line) of the M_2 ellipse at Gibraltar's main sill. Negative values of the semiminor axis indicate that the M_2 current turns clockwise. Also indicated are extremum values observed for the semiminor axis in each layer of specific rotation.

value the 2.1 Sv for the rms of tidal transport deduced earlier from mode 1 of the tidal currents (Figure 6*a*), which is based mostly on deep layer measurements, might be an underestimation.

The phase of the M_2 flood current (Figure 11, dashed line), presents earlier phases toward the bottom and sides of the section. This is in accordance with the presence of frictional boundary layers on a channel flow forced by a periodic pressure gradient [*Yasuda*, 1987]. The M_2 current occurs ~ 40 min in time earlier at the bottom than at the surface center of the section. The mean phase of 145° at ~ 200-m depth agrees well with that obtained from a pressure difference across the strait between DS and DN stations assuming a geostrophic balance, before correcting for their internal tide contribution (Appendix A). From the shallow pressure sensors (SS-SN), the M_2 current phase at the surface average across the strait is 129°. This surface phase is reasonable considering the large portions of shallow shelves at the north and south sides of the sill section, which should have tidal current phases appreciably earlier than those at the center of the strait.

The orientation of the M_2 tidal ellipses (Figure 12, dashed line) are indicative of a convergent flow conforming to the local topography. At the center of the sill section in the vertical, a clockwise rotation of the orientation occurs as one moves up in the water column, in accordance with the way a steady current rotates in a frictional Ekman boundary layer. However, *Yasuda's* [1987] linear model for the vertical structure of a tidal current in an ocean with lateral boundaries indicates an opposite sense of rotation for the orientation in the vertical. That is, in his model, which assumes a constant eddy viscosity, the ellipse's orientation bears anticlockwise moving up in the water column from the bottom. One would be tempted to attribute this discrepancy with the theory, to local topographic and nonlinear effects around moorings M2 and M3. The point is that most of the current observations described in this paper (Table 2) and in other straits [*Godin et al.*, 1981], indicate that the orientation of the major axis bears to the right (clockwise in the northern hemisphere) as one moves up in the water column. Although it will not be pursued here, it is clear that the available model for the vertical structure of the tidal currents in the presence of lateral boundaries needs to be critically reviewed on this point.

The semiminor axis of the M_2 current ellipse (Figure 12, solid line) indicates a nearly rectilinear current in the strait. The sign of

this parameter is related to the sense of rotation of the tidal current, showing clockwise currents at depths < 200 m that become counterclockwise toward the bottom, a characteristic related to the effects of a bottom boundary layer and predicted by linear theory [*Prandle*, 1982; *Yasuda*, 1987].

The vertical dependence of the tidal ellipse parameters is a clear indication of the effects of friction and, in principle, should permit a way of evaluating its order of magnitude. From time dependent Ekman layer theory in an unbounded ocean [*Prandle*, 1982], the vertical decay scale (δ_+) for the counterclockwise rotating tidal current component R_+ of frequency ω is $\delta_+ = \sqrt{2A/(f+\omega)}^{-1}$, where A is a constant vertical eddy viscosity coefficient and f is the Coriolis parameter. By fitting the theoretical vertical profile for R_+ at the M_2 frequency to that observed at the M2 central sill mooring location, a value of $\delta_+ \sim 110$ m is obtained. This vertical decay scale gives an eddy viscosity $A \sim 1.4$ m^{2}s^{-1}, which implies strong internal stresses related to an e-folding time τ of ~ 3.6 hours. *Thompson et al.* [1989], on the basis of a pilot mooring kept for ~ 15 days on a northern sill location in June 1984, estimated values of $\delta_+ \sim 60$ m, $A \sim 0.4$ m^{2}s^{-1}, and $\tau \sim 5.6$ hours. The two estimates differ appreciably but, nevertheless, fall within the bottom intensified dissipation rates obtained around the strait's sill by *Wesson and Gregg* [1987], which imply a range for τ between 3 and 30 hours if a characteristic tidal current velocity of 1 m s^{-1} is assumed.

5. The Mediterranean and the Atlantic Tide

The tides in the Mediterranean result from the interaction of direct tidal forcing within the sea and the co-oscillating tide coming in from the Atlantic through Gibraltar. *Defant* [1961] reviews earlier work on the tidal motion in the Mediterranean. In this section, order of magnitude estimates, disregarding rotational effects, will be set forth to get a conceptual idea of how much of the observed tide is directly forced and what is the extent of influence of the tide entering from the Atlantic.

To estimate the effect of astronomic forcing, the Mediterranean will be represented as a uniform channel centered around the 36°N latitude, with a length of 3800 km and a mean depth of 1500 m. The tidal forces due to M_2 at a latitude of 36°N has a magnitude of $3\ GMa \sin\theta/2r^3 = 6.91\ 10^{-5}$ dyn g^{-1} (where G is Newton's gravitational constant, M is the mass of the Moon, a is the mean radius of the Earth, r is the mean Earth-Moon distance, and θ is the colatitude of the channel axis). This force will be considered constant over the channel domain, since the M_2 satellite ($\sigma = 28.98°/\text{h}^{-1}$) takes less than 2 hours to traverse the whole sea.

The linear momentum and continuity equations for a one-dimensional forced frictionless fluid in a channel are

$$\frac{\partial u}{\partial t} = -g\frac{\partial \eta}{\partial x} + T_o \exp^{i\sigma t} \tag{1}$$

$$H\frac{\partial u}{\partial x} = -\frac{\partial \eta}{\partial t} \tag{2}$$

where u is the velocity component in the x direction, η is the surface elevation, T_o is the magnitude of the forcing function at frequency σ, and g is the acceleration due to gravity.

Taking the fluid response as also periodic with the same frequency as the forcing, i.e., $u, \eta \propto \exp(i\sigma t)$, we get

$$i\sigma u = -g\frac{\partial \eta}{\partial x} + T_o \tag{3}$$

$$H\frac{\partial u}{\partial x} = -i\sigma\eta \tag{4}$$

an equation for η is then

$$\frac{\partial^2 \eta}{\partial x^2} - k^2\eta = 0 \quad k = \frac{\sigma}{\sqrt{gh}} \tag{5}$$

which has general solutions

$$\eta = \left[A \exp^{-ikx} + B \exp^{ikx}\right] \exp^{i\sigma t} \tag{6}$$

$$u = \sqrt{\frac{g}{H}}\left[A \exp^{-ikx} - B \exp^{ikx}\right] \exp^{i\sigma t} + \frac{T_o \exp^{i\sigma t}}{i\sigma} \tag{7}$$

For a channel closed at $x = \pm\frac{1}{2}L$, where L is the length of the channel, the boundary conditions to be satisfied are $u(\frac{1}{2}L) = u(-\frac{1}{2}L) = 0$. Upon substituting in the solution for u, it is found that

$$A = -B \quad A = \frac{iT_o}{2gk\cos kL/2} \tag{8}$$

which gives [*Godin*, 1989]

$$\eta = \frac{T_o}{gk}\frac{\sin kx}{\cos kL/2}\exp^{i\sigma t} \quad u = \frac{T_o}{\sigma}\left[1 - \frac{\cos kx}{\cos kL/2}\right]\exp^{i(\sigma t - \pi/2)} \tag{9}$$

When appropriate numerical values for the Mediterranean case are used, the amplitude for the directly forced tide is obtained as

$$\left|\eta_{M_2}\right| = \left|\frac{T_o}{g\,k\cos(kL/2)}\right| = 10.3 \text{ cm} \tag{10}$$

This value is very close to that observed in many places within the Mediterranean [*Defant*, 1961, p. 392], which implies that there should be little contribution from the Atlantic cooscillating tide entering through Gibraltar, to the tide in the sea.

To get an idea of how constrictive the strait is to an incoming tidal wave from the Atlantic, the Gulf of Cadiz is represented by a rectangular channel, 350 km wide and 730 m deep, that abruptly connects to the strait, supposed 24.5 km wide and 120 m deep. The amplitude ratio of a reflected (g) to an incident (f) wave at the junction between the two channels is [*Lighthill*, 1978, chapter 2] $g/f = (Y_1 - Y_2)/(Y_1 + Y_2)$, where Y_1 and Y_2 are the admittances of the gulf (1) and the strait (2), $Y_i = A_i/(\rho_i c_i)$ (A_i being the cross-sectional area, ρ_i the fluid density, and c_i the wave velocity in channel i). To arrive at this relation of g/f, continuity of pressure due to the waves ($f+g = h$, where h is the transmitted wave) and volume transport ($Y_1(f-g) = Y_2 h$) at the junction are both specified. This calculation indicates that about 94% of the incident Atlantic wave gets reflected at the mouth of the strait.

The amplitude ratio of transmitted (h) to incident (f) waves at the entrance to the Mediterranean can be obtained, given that the Alboran Sea, east of the strait, can be modeled as a channel 87 km wide and about 570 m deep. *Lighthill* [1978] shows that $h/f = 2Y_1/(Y_1 + Y_2)$, indicating that the amplitude of the tidal wave entering the Mediterranean is reduced to 0.24 times its value in the strait. Even though a further reduction is expected as the wave travels east, this amplitude is not negligible. In order to further illustrate the role of the Atlantic tide in the Mediterranean, it is useful to evaluate the volume of water incident east of the sill

during half a tidal cycle. M_2 has a volume transport amplitude of 2.6 Sv at the sill which corresponds to a volume of 3.7×10^{10}m^3 over a flood cycle. The horizontal area of the Mediterranean is 2.5×10^{12}m^2, so the transport due to M_2 through the strait corresponds to a uniform rise of 1.4 cm, or near 10% of the amplitude of the directly forced M_2 tide.

Neglecting the effect of astronomical forcing and Earth tides, the time mean energy flux associated with a sinusoidal variation of elevation amplitude η, with phase ϕ and current amplitude U, with phase θ is $\frac{1}{2}\rho g \eta U \cos(\phi-\theta)$ [*Robinson*, 1979]. This flux must be integrated over a vertical plane normal to the current direction to obtain the total energy flux transport. The phase difference between the elevation and the current is a determinant factor of the energy flux. The logical place to measure energy flux through the strait is its main sill, and as was pointed out in a previous section, the principal tidal pressure and current fields are 90° out of phase there. This implies expecting a near-zero tidal energy flux to occur through the strait. Using the 25-point measurements of currents available from M1, M2, M3, and F3, an estimate of surface currents from the pressure difference between SS and SN, and the bottom pressure information in the area, it is possible to estimate the energy flux due to the M_2 tide. An average of 276 ± 367 W m^{-2} is obtained, which when multiplied by the sill's cross-sectional area gives a net M_2 tide energy flux of $8\ 10^5 \pm 10^6$ kW. Even though the mean is positive, indicative of a net inward energy flux, the standard deviation renders it statistically unreliable, confirming the earlier supposition of a nearly zero net flux. An interesting consequence of this result is that whatever net work the tidal potential is doing on the water of the Mediterranean, this energy must be dissipated within the sea. A detailed evaluation of the tidal energy budget in the Mediterranean would be very much worthwhile, since besides frictional dissipation, some of the energy from the tide might be feeding part of the energetic low-frequency circulation observed in the sea, possibly through mixing and tidal rectification mechanisms.

6. CONCLUSIONS

The observations described here show that the M_2 tide has a complicated structure in the strait: the local cotidal chart reveals a large gradient in the amplitude of the tide, and the phase appears to increase with distance from the southern tip of Spain. Tidal currents reach large amplitudes relative to subinertial or mean flows. At the sill, the tidal currents often reverse the direction of the flow expected from the steady exchange between Atlantic and Mediterranean waters. The structure of tidal currents is principally barotropic, and the interface between the two water masses exhibits large vertical excursions at the tidal periods. The vertical displacements of the interface are locked in phase with the sea surface at the sill, suggesting that the area acts to generate internal tides.

The Atlantic tide forces motions within the strait, and tidal mass transport suggests that it could account for 10% of the tidal motions in the Mediterranean basin. The phase relation between pressure and currents correspond to that of a standing wave, and estimates of energy flux are within error of zero.

Oscillating transports in each layer, computed at the sill from currents and the varying cross-section of the layer, are large, of the order of 2 Sv. These calculations suggest that at tidal frequencies the interface acts as a membrane between the two water masses: when Atlantic water floods into the strait, the interface is depressed and Mediterranean water is forced back toward the east. A half cycle later, the lower layer flowing back forces the interface toward the surface, and the Atlantic water ebbs back to the west. The correlation between fluctuating quantities which make up the transport are significant, leading to a mean transport in the upper layer of 0.21 Sv toward the east, and a mean return in the lower layer of 0.17 Sv, i.e., in the same direction as the mean, density-driven, exchange flows. This result emphasizes the importance of computing mean transports as a correlation between fluctuating quantities, rather than as the product of the average velocity by the average cross- section of each layer.

The structure of the cotidal chart can be explained in terms of simple momentum arguments. To first order, a balance exists in the along-strait direction between local acceleration and the pressure gradient, while in the perpendicular direction a geostrophic balance is observed. The surface pressure gradient is large compared with baroclinic gradients, so the resulting flow is mainly barotropic.

The role of friction in the momentum balance can be parameterized with a linear friction coefficient λ. Various ways of estimating λ imply a numerical value between 1.8×10^{-5}s^{-1} and 5×10^{-5}s^{-1}. A frictional model of the vertical structure of the tidal currents leads to an estimate of eddy viscosity $A_v = 1.4$ m^2 s^{-1}. These estimates of friction are comparable, corresponding to a friction decay time scale ranging between 3 and 16 hours. A further study of the detailed behavior of higher tidal harmonics, which can be related to friction, might shed further light on the role of friction and dissipation.

APPENDIX A: INTERNAL TIDE CONTRIBUTION TO BOTTOM PRESSURE

In the strait there exists a well-defined two-layer flow over variable topography, with a high density contrast between the layers. In the presence of strong forcing at both subinertial and tidal frequencies, large fluctuations of the interface are to be expected and are observed. *Lacombe and Richez* [1982] report observations of tidal excursions of the interface near 100 m in amplitude. To estimate the contribution such excursions can have on pressure observations made at the bottom, consider a 300-m-depth column of water separated in two by an interface with a relative density difference of $2\,\sigma_t$. A 100-m fluctuation of the interface will produce a bottom pressure fluctuation of about 20 mbar. This corresponds to 1/6 to 1/5 of the M_2 component of bottom pressure measured near the sill. To define surface tidal fluctuations using pressure observations made at the bottom beneath the interface, it is necessary to separate the contribution of interfacial fluctuations from the pressure observations. A 50-m internal tide would imply distortions of up to 10 mbar in amplitude and ± 11° in phase of the surface constituent at any given frequency, depending on the relative phase between the internal and the surface tide. The internal tide propagation speed depends on the depth of the interface as well as fluctuations in the density field. Thus it could be argued that away from an internal tide generation area the phase relation between the internal tide and surface tide would be random. In that case, a direct harmonic analysis of a reasonably long bottom pressure series would tend to average out the internal tide contribution and approximate well the amplitude and phase of the surface tide constituents. How far from the generation region is enough to insure this to be true cannot be precisely determined and needs to be critically examined at any location where bottom pressure is measured. This distance is likely to be shorter where interface depths and/or density variations are large and where mixing is important, since all these processes affect the internal tide phase speed. Rather than describing the internal tide and how

it is generated and propagates through the strait, we are principally concerned here with describing the pressure and current field at tidal frequencies due to the surface tide in the strait. In this regard, the internal tide contribution to pressure represents an unwanted signal which needs to be eliminated from deep bottom pressure measurements. With knowledge of the vertical density profile over an instrumented site as a function of time, the hydrostatic equation can be used to remove the baroclinic component of the pressure fluctuation. In locations where mixing is not very important and where a stable relation between temperature and salinity ($T-S$) is observed, a continuously measured density profile can be approximated by temperature observations, as obtained for instance with a thermistor chain [*Merrifield and Winant*, 1989]. In the Strait of Gibraltar, mixing tends to make the $T-S$ relation vary in time, and thus in order to have reasonable estimates of the vertical density profile, simultaneous measurements of temperature and salinity are required.

For observations made at the sill the fluctuating density struc-

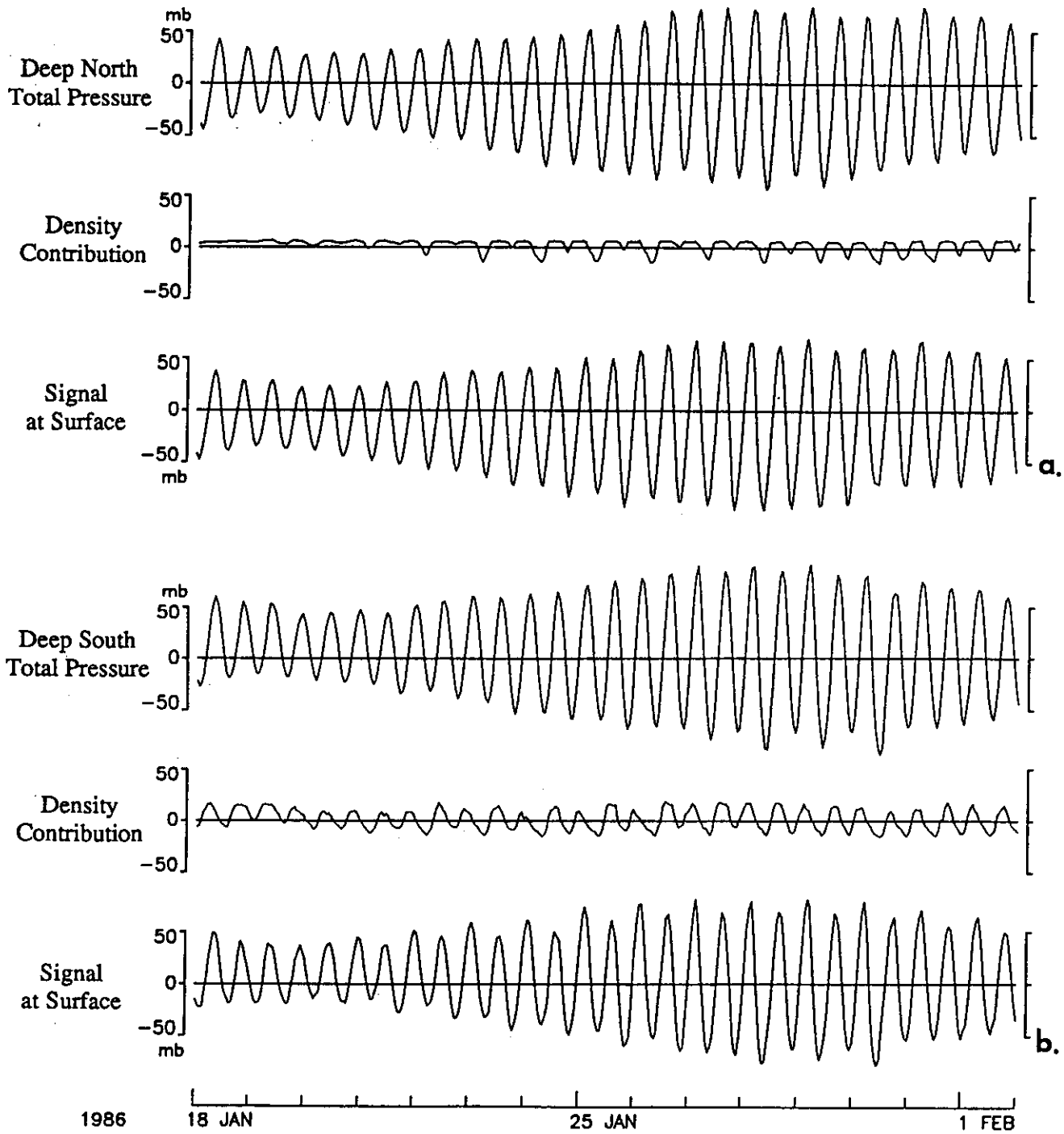

Fig. 13. (top) The bottom recorded pressure, (middle) the pressure due to the varying weight of the column of water, and (bottom) the difference of the two "Signal at surface," for the two deep sill stations (*a*) Deep North and (*b*) Deep South. The total available series cover the period from October 26, 1985, to March 11, 1986, for DN and October 27, 1985, to March 21, 1986, for DS, but only the 15-day period from January 18 to February 2, 1986, is shown for clarity.

TABLE 8. Principal Tidal Constituents for Pressure Sensors DS and DN

Constituent	Total Pressure Amplitude, mbar	Total Pressure Phase, deg	Weight of Column Contribution Amplitude	Weight of Column Contribution Phase	Signal at Surface Amplitude	Signal at Surface Phase
			Deep North (DN) (3257 Hours)			
O_1	3.2	245.8	2.4	219.7	1.5	291.7
K_1	1.6	14.0	2.2	301.2	2.5	83.3
M_2	62.9	47.0	5.9	348.3	60.1	51.8
S_2	23.5	70.9	1.5	24.2	22.5	73.8
			Deep South (DS) (3459 Hours)			
O_1	2.3	275.9	2.6	205.5	2.8	335.7
K_1	2.3	55.0	2.3	277.4	4.4	76.3
M_2	62.5	53.9	11.7	14.6	54.0	61.8
S_2	23.2	78.7	2.8	42.0	21.1	83.3

Principal diurnal (O_1 and K_1) and semidiurnal (M_2 and S_2) tidal constituents for the bottom pressure measurements at Deep North and Deep South stations. Three values are given for each constituent: The first (total pressure) correspond to the constituents obtained by direct analysis on the raw bottom pressure records. The second (weight of column contribution) are the harmonic constants of the fluctuations of the weight of the water column above each instrument, obtained as explained in the text. The third (signal at surface) are harmonic estimates of the pressure records once the contribution of the fluctuating weight of the water column has been removed from the raw bottom pressure record. All estimates are based on direct harmonic analysis of the records whose length is indicated beside the station name. Inference has been used to separate the contribution of P_1 to K_1 and K_2 to S_2 from their relation at Cadiz. Phases are in degrees with respect to GMT.

ture can be estimated from current meter observations of salinity and temperature. Mooring M1 was located 2 km away from bottom pressure station DN, where the depth was 210 m, and the density and depth records for instruments at 143 m, 156 m, and 167 m are available. The density at the surface is taken as that measured by the SN sensor, measured inshore of DN, near the surface, and the density at the bottom is recorded by the DN instrument. With these five records and interpolating linearly between points, an estimate of the time-varying weight of the water column, due to density variations is obtained. DS is also in 210-m water depth, on the south side of the sill, and situated 1 km away from mooring M3, where three instruments were located at 110 m, 140 m, and 180 m. There were no continuous surface density measurements available nearby; however, conductivity-temperature-depth (CTD) yo-yo stations in the vicinity of DS have shown a nearly constant surface value of density of $26.8 \pm 0.15\ \sigma_t$, over a period exceeding 12 hours during spring tides [*Bray*, 1986]. Variations in the weight of the column of water over DS, due to density fluctuations, are therefore estimated using a constant value of density of $26.8\ \sigma_t$ at the surface, density measurements at the three current meters on M3 and the density measured at the pressure instrument DS.

The results of these calculations, for locations DN and DS, are illustrated in Figures 13*a* and 13*b*. The top frame in each figure corresponds to the measured bottom pressure. The middle frame illustrates variations due to the changes in the weight of the water column over the instrument. The difference between these two is the pressure at the surface, shown in the bottom frame. This pressure is not due solely to the surface tide, since the internal tide can have a signature at the surface in the pressure field [*Gill*, 1982; p. 122]. The internal contribution to the surface pressure should be small, however, and more importantly, by removing the density contribution to bottom pressure records those records become comparable to pressure measurements made near the surface.

The amplitude and phase of the main tidal constituents in the diurnal (O_1 and K_1) and semidiurnal (M_2 and S_2) bands are summarized in Table 8, for each of the time series shown in Figures 13*a* and 13*b*. The analyses considered the total length of the time series indicated in the table and not only the portions shown in the figures. Inference [*Godin*, 1972] has been used to separate the contributions of P_1 to K_1 and K_2 to S_2. Sea level observations at Cadiz, which extend over a very long time period, have been used for this. Observations reported by *Lacombe and Richez* [1982] and by *Bray* [1986] suggest that the largest excursions of the interface occur on the southern side of the sill near station DS. The values indicated for this station in Table 8 thus represent an upper limit for internal contributions of the deep bottom pressure measurements anywhere inside the strait. Based on those observational reports it seems safe to assume that the internal contribution at stations DW and DP5, which cannot be measured directly, is substantially less than those observed at DN.

Results summarized in Table 8 show that the surface and internal amplitudes are of the same order at the diurnal frequencies, implying that with the available observations it is not possible to identify one contribution from the other. This explains in part the erratic behavior of the diurnal constituents that has been observed in the sea level and bottom pressure records throughout the strait [*García et al.*, 1987]. In this paper, the corrected DN and DS series are used in all the calculations. Series at DW and at DP5 are used as measured with the assumption that the internal contributions are unimportant at these locations.

APPENDIX B: NOTE ON ADMITTANCE ESTIMATES OF CURRENT SERIES

Admittance calculations [*Godin*, 1978] consist of computing cross spectra between a nearby vertical tide station (pressure or sea level) taken as input and each of the horizontal current components as outputs. The spectral structure of the vertical tide station chosen should be well known, by which it is meant that reliable, statistically stable, and well-resolved estimates of the main tidal constituents for the site are available. One basic assumption

of the method is that since the vertical tide and horizontal tidal currents, in a given region, are integral parts of the same phenomena, the amplitude ratios and phase differences between the major tidal constituents within a given tidal band (diurnal or semidiurnal) are the same in the vertical tide and in the current components. If this is the case, cross spectra can be calculated with a broadband frequency resolution of 1 cpd. This has the desirable property of more statistical stability in comparison with a finer resolution, but it is still possible to resolve specific constituents within a tidal band in the output series by assuming that the admittance function (defined as the complex ratio of the cross-spectra over the power spectra of the input) is constant throughout the band. Using nearby tidal stations within the region of study as input is more sensible than using the astronomical tidal potential. It is likely that specific basin response will alter the spectral structure of the original astronomical tidal forcing and render the constant admittance assumption for a given tidal band useless. The assumption of similar spectral structure for the vertical and current tidal records within a region is reasonable, and when the length and quality of the current records have permitted reliable and well-resolved estimates of the tidal constituents, it has been proven to hold true [*Godin and Gutierrez*, 1986]. In the strait, when with direct harmonic analysis of the currents, S_2 is resolved directly from K_2, it is found that the ratio of amplitudes of M_2/S_2 (semimajor axis of their constituent ellipses) and phase differences $\theta S_2 - \theta M_2$ are ~ 2.7° and ~ 26°, respectively, which are the same as found for example at the pressure stations of Ceuta and Deep North. This main assumption breaks down when a node for a given constituent is present between the vertical tide station and the current measurement location used. This could be the case in relation to the diurnal constituents O_1 and K_1, which seem to have differing amplitude ratios and phase differences between the east and west ends of the strait, as was discussed earlier. In such a situation the sea level station used as reference in the admittance calculations, should be as close as possible to the current observations to reduce the risk of having a node in between.

Acknowledgments. The work described here is part of the Gibraltar Experiment. The authors wish to express their appreciation to their Spanish and Moroccan colleagues and the various field groups who made the experiment so successful. Special thanks are due to Harry Bryden, from WHOI, and David Farmer, from IOC, for providing their current meter data, and Neal Petigrew, from UNH, for supplying pressure data from his Tarifa South (DP5) station. Tangier's Port Captain, Commandant El Affaqui, is greatly thanked for his invaluable help during the experiment. We are indebted to Joan Semler for carefully typing this paper and Mike Clark for the artwork. This work was supported by the Office of Naval Research under contract N00014-85-C-0223.

REFERENCES

Armi, L., and D. M. Farmer, The Flow of Mediterranean Water through the Strait of Gibraltar, *Prog. Oceanogr., 21*(1), 1–105, 1988.

Bormans, M., C. Garrett, and K. R. Thompson, Seasonal variability of the surface inflow through the Strait of Gibraltar, *Oceanol. Acta, 9*, 403–414, 1986.

Bray, N. A., Gibraltar Experiment CTD data report, *SIO Ref. 86-21*, 212 pp., Scripps Inst. of Oceanogr., La Jolla, Calif., 1986.

Bryden, H. L., and H. M. Stommel, Limiting processes that determine basic features of the circulation in the Mediterranean Sea, *Oceanol. Acta, 7*, 289–296, 1984.

Bryden, H. L., E. C. Brady, and R. D. Pillsbury, Flow through the Strait of Gibraltar, paper presented at the Gibraltar Symposium, Madrid, October 24–29, 1988.

Candela, J., and G. Godin, Structure of the currents measured across a section of Johnstone Strait, Canada, *Cont. Shelf Res., 9*(1), 1–17, 1989.

Candela, J., C. D. Winant, and H. L. Bryden, Meteorologically forced subinertial flows through the Strait of Gibraltar, *J. Geophys. Res. 94*(C9), 12,667–12,679, 1989.

Defant, A., *Physical Oceanography*, vol. I, 729 pp., Pergamon, New York, 1961.

Farmer, D. M., and L. Armi, Maximal two-layer exchange over a sill and through the combination of a sill and a contraction with barotropic flow, *J. Fluid Mech., 164*, 53–76, 1986.

Farmer, D. M., and L. Armi, The flow of Atlantic Water through the Strait of Gibraltar, *Prog. Oceanogr., 21*(1), 1–105, 1988.

Flagg, C. N., J. A. Vermersch, and R. C. Bearsdley, M.I.T. New England shelf dynamics experiment (March, 1974) data report, II, The moored array, *Rep. 76-1*, Dep. of Meteorol., Mass. Inst. of Technol., Cambridge, 1976.

Forsythe, G. E., M. A. Malcom, and C. B. Moler, *Computer Methods for Mathematical Computations*, xi + 259 pp., Prentice Hall, Englewood Cliffs, N.J., 1977.

García La Fuente, J., F. de Castillejos, and M. J. García, Resultados de la red mareográfica en el Estrecho de Gibraltar, *Rev. Geofis., 43*, 37–56, 1987.

Garrett, C., and B. Petrie, Dynamical aspects of the flow through the Strait of Belle Isle, *J. Phys. Oceanogr., 11*(3), 376–393, 1981.

Garrett, C., J. Akerley, and K. Thompson, Low-frequency fluctuations in the Strait of Gibraltar from MEDALPEX sea level data, *J. Phys. Oceanogr., 19*(11), 1682–1696, 1989.

Gill, A. E., *Atmosphere-Ocean Dynamics, Int. Geophys. Ser.*, vol. 30, xv + 662 pp., Academic, San Diego, Calif., 1982.

Godin, G., *The Analysis of Tides*, xxi + 264 pp., University of Toronto Press, Toronto, Ont., Canada, 1972.

Godin, G., The use of the admittance function in the reduction and interpretation of tidal records, *Manuscr. Ser. 41*, 46 pp., Marine Environmental Data Service, Ottawa, Ont., Canada, 1976.

Godin, G., L'analyse des donnees de courants: Théorie et practique, *Manuscr. Ser. 49*, 91 pp., Marine Environmental Data Service, Ottawa, Ont., Canada, 1978.

Godin, G., *Tides*, Centro de Investigación Científica y Educación Superior de Ensenada, Ensenada, Mexico, in press, 1989.

Godin, G., and J. Candela, Tides and currents in Fury and Hecla Strait, *Estuarine Coastal Shelf Sci., 24*, 513–525, 1987.

Godin, G., and G. Gutierrez, Non-linear effects in the tide of the Bay of Fundy, *Cont. Shelf Res., 5*(3), 379–402, 1986.

Godin, G., J. Candela, and R. de la Paz, An analysis and interpretation of the current data collected in the Strait of Juan de Fuca, *Mar. Geod., 5*(3), 273–302, 1981.

Hendershott, M. C., Ocean Tides, *Eos Trans. AGU, 54*, 76–86, 1973.

Hibiya, T., Generation mechanism of internal waves by tidal flow over a sill, *J. Geophys. Res., 91*(C6), 7697–7708, 1986.

Kinder, T. H., and H. L. Bryden, The 1985–1986 Gibraltar Experiment: Data collection and preliminary results, *Eos Trans. AGU, 68*, 786, 1987.

Kundu, P. K., J. S. Allen, and R. L. Smith, Modal decomposition of the velocity field near the Oregon coast, *J. Phys. Oceanogr., 5*, 683–704, 1975.

Lacombe, H., and C. Richez, The regime of the Strait of Gibraltar, in *Hydrodynamics of Semi-Enclosed Seas*, edited by J. C. J. Nihoul, pp. 13–74 pp., Elsevier, Amsterdam, 1982.

Lighthill, M. J., *Waves in Fluids*, xv + 504 pp., Cambridge University Press, 1978.

Merrifield, M. A., and C. D. Winant, Shelf circulation in the Gulf of California: A description of the variability, *J. Geophys. Res., 94*(C12), 18,133–18,160, 1989.

Pillsbury, R. D., D. Barstow, J. S. Bottero, C. Milleiro, B. Moore, G. Pittock, D. C. Root, J. Simpkins III, R. E. Still, and H. L. Bryden, Gibraltar Experiment, Current measurements in the Strait of Gibraltar, October 1985–October 1986, *OSU Data Rep. 87–29, Ref. 139*, 284 pp., Coll. of Oceanogr., Oreg. State Univ., Corvallis, 1987.

Prandle, D., The vertical structure of tidal currents, *Geophys. Astrophys. Fluid Dyn., 22*, 29–49, 1982.

Robinson, I. S., The tidal dynamics of the Irish and Celtic seas. *Geophys. J. R. Astron. Soc., 56* 159–197, 1979.

Rocha, C., and A. J. Clarke, Interaction of ocean tides through a narrow single and narrow multiple strait, *J. Phys. Oceanogr., 17*(12), 2203–2218, 1987.

Sección de Oceanografía, *Anuario de Mareas*, 139 pp., Instituto Hidrográfico de la Marina, Cadiz, Spain, 1986.

Thompson L., T. Kinder, and H. L. Bryden, Flow on the sill in the Strait of Gibraltar, paper presented at Workshop on the Physical Oceanography of the Strait of Gibraltar, Madrid, Spain, Oct. 24–28, 1988, 1989.

Wesson, J. C., and M. C. Gregg, Turbulent dissipation in the Strait of Gibraltar and associated mixing, in *Small-Scale Turbulence and Mixing in the Ocean*, edited by J. C. J. Nihoul and B. M. Jamart, pp. 201–212, Elsevier, New York, 1987.

Wunsch, C., Internal tides in the ocean, *Rev. Geophys.*, *13*(1), 167–182, 1975.

Yasuda, H., Vertical structure of the tidal current ellipse in a rotating basin, *J. Oceanogr. Soc. Jpn.*, *43*, 309–318, 1987.

J. Candela and C. Winant, Scripps Institution of Oceanography, La Jolla, CA 92093.

A. Ruiz, Sección de Oceanografía, Instituto Hidrográfico de la Marina, 11007 Cadiz, Spain.

(Received July 5, 1989;
accepted August 22, 1989.)